DYNAMICAL PRUNING OF ROOTED TREES WITH APPLICATIONS TO 1D BALLISTIC ANNIHILATION

YEVGENIY KOVCHEGOV AND ILYA ZALIAPIN

ABSTRACT. We introduce *generalized dynamical pruning* on rooted binary trees with edge lengths that encompasses a number of discrete and continuous pruning operations, including the tree erasure and Horton pruning. The pruning removes parts of a tree T, starting from the leaves, according to a pruning function defined on descendant subtrees within T. We prove the invariance of critical binary Galton-Watson tree with exponential edge lengths with respect to the generalized dynamical pruning for an arbitrary admissible pruning function. These results facilitate analysis of the continuum 1-D ballistic annihilation model $A + A \to \varnothing$ for a constant particle density and initial velocity that alternates between the values of ± 1. We show that the model's shock wave is isometric to the level set tree of the potential function, and the model evolution is equivalent to the generalized dynamical pruning of the shock wave tree.

CONTENTS

1. Introduction

Pruning of tree graphs is a natural operation that induces a contracting map [28] on a suitable space of trees, with the empty tree ϕ as the fixed point. Examples of prunings studied in probability literature include erasure from leaves at unit speed [38, 21, 15], cutting the leaves [14, 31, 33], and eliminating nodes/edges at random [5, 1]. A recent survey of random tree measures invariant with respect to cutting the leaves is given in [34].

1.1. Generalized dynamical pruning.

We consider here the erasure of a tree from the leaves down at a non-constant tree-dependent rate. Specifically, we introduce *generalized dynamical pruning* $\mathcal{S}_t(\varphi, T)$ of a rooted tree T that eliminates all subtrees $\Delta_{x,T}$ (defined as the points descendant to point x in T) for which the value of a function $\varphi(\Delta_{x,T})$

is below t (see Sect. 3 for a formal definition). The generalized dynamical pruning encompasses a number of discrete and continuous pruning operations, depending on the choice of function φ. For instance, the tree erasure from leaves at unit speed [38, 21, 15] corresponds to the pruning function $\varphi(T)$ equal to the height of T; and the Horton pruning [14, 33] corresponds to $\varphi(T)$ equal to the Horton-Strahler order of T. For most selections of $\varphi(T)$, the map induced by the generalized dynamical pruning does not have a semigroup property, which distinguishes it from the operations studied in the literature.

In Sect. 4.3, Thm. 2 we establish invariance of the space of critical binary Galton-Watson trees with i.i.d. exponential edge lengths with respect to the generalized dynamical pruning, independently of (an admissible) pruning function. The invariance includes scaling of the edge lengths by the scaling constant equal to the survival probability $\mathsf{P}(\mathcal{S}_t(\varphi, T) \neq \phi)$. The explicit form of the survival probability is established in Thm. 3 for pruning by tree height (erasure from leaves at unit speed), by Horton order, and by tree length. The generalized prune invariance unifies several known invariance results (e.g., [38, 14]) and suggests a framework for studying diverse problem-specific pruning operations.

As a notable application, we consider the 1-D ballistic annihilation model and show that its dynamics can be represented as a generalized dynamical pruning of the level set tree of the model potential (Sects. 5,6).

1.2. **Ballistic annihilation model.** The ballistic annihilation model, traditionally denoted $A + A \to \varnothing$, describes the dynamics of particles on a real line: a particle with Lagrangian coordinate x moves with the velocity $v(x, 0)$ until it collides with another particle, at which moment both particles annihilate, hence the model notation. The annihilation dynamics appears in chemical kinetics and bimolecular reactions; see [18, 7, 9, 41, 17, 8, 19, 13, 35, 44].

The annihilation dynamics produces *sinks* (*shocks*) that correspond to the collisions of individual particles with consequent annihilation. The moving *shock waves* represent the *sinks* that aggregate the annihilated particles and hence accumulate the mass of the media. Dynamics of these sinks resembles a coalescent process that generates a tree structure for the sink trajectories; we call it a *shock wave tree*. The dynamics of a ballistic annihilation model with two coalescing sinks is illustrated in Fig. 1.

1.3. **Ballistic annihilation with two valued initial velocity.** In Sect. 6 we consider a model on a finite interval $[a, b]$ with a constant

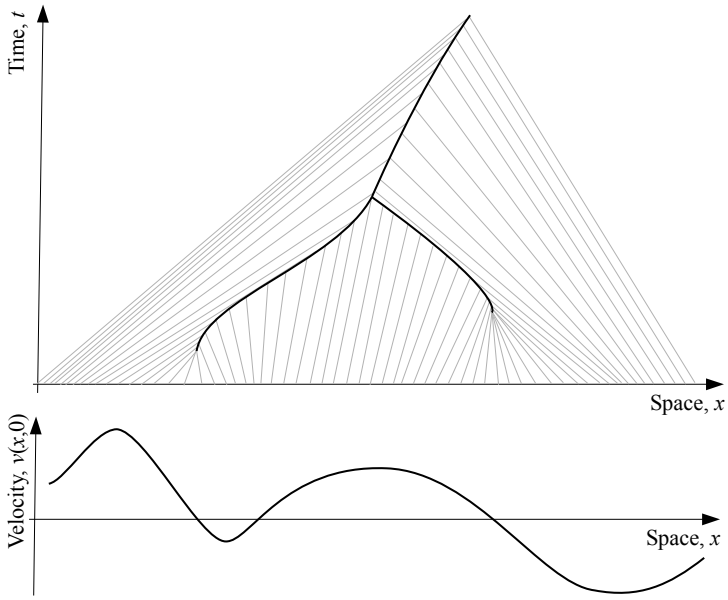

FIGURE 1. Ballistic annihilation model: an illustration. A particle with Lagrangian coordinate x moves with velocity $v(x,0)$ until it collides with another particle and annihilates. (Bottom panel): Initial velocity $v(x,0)$. (Top panel): The space-time portrait of the system. The trajectories of selected particles are depicted by gray thin lines. The shock wave that describes the motion and coalescence of sinks is shown by solid black line. The sink trajectory in this example forms an inverted Y-shaped tree.

initial particle density $g(x,0) = g_0$ and an initial velocity field $v(x,0)$ that alternates between the values ± 1, as illustrated in Fig. 2. Equivalently, we work with potential velocity field $v(x,t) = -\partial_x \psi(x,t)$ where the initial potential $\Psi_0(x) = \psi(x,0)$ is a piece-wise linear continuous function with slopes ± 1. We furthermore assume that $\Psi_0(x)$ is a negative excursion on $[a,b]$. This choice corresponds to a particularly tractable structure of the shock wave tree, which is completely described in this work. In particular, the combinatorial structure and planar embedding of the shock wave tree coincides with that of the level set tree $T = \text{LEVEL}(\psi(x,0))$ of the initial potential (Sect. 6, Thm. 4).

1.4. **Ballistic annihilation as dynamical pruning.** The main applied result of our work (Sect. 6, Thm. 6) states that the ballistic annihilation dynamics in case of a unit slope potential is equivalent to

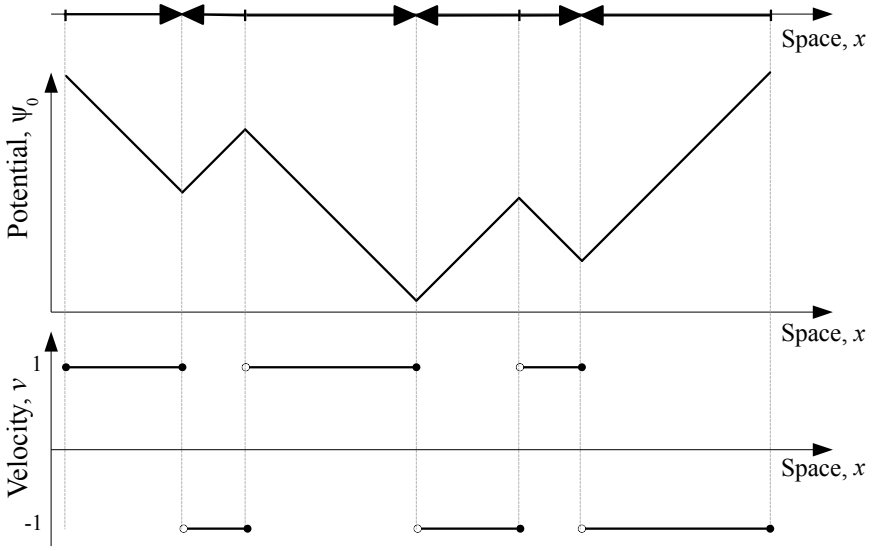

FIGURE 2. Piece-wise linear unit slope potential: an illustration. (Top): Arrows indicate alternating directions of particle movement on an interval in $\mathbb{R}$. (Middle): Potential $\Psi_0(x)$ is a piece-wise linear unit slope function. (Bottom): Particle velocity alternates between values ± 1 within consecutive intervals.

the generalized dynamical pruning of the shock wave tree with pruning function $\varphi(\tau)$ equal to the total length of τ.

The pruned tree in this construction describes the potential restricted to the domain of particles that did not annihilate until instant t. To retain information about sinks and empty intervals, we equip a tree with *massive points*, placed at the tree *cuts* – the boundary of the pruned tree parts (Sect. 6.4, Def. 3). A complete description of ballistic annihilation dynamics is then given in terms of mass-equipped trees, which involves a suitably modified definition of pruning (Sect. 6.4). In particular, we establish a one-to-one correspondence between pruned mass-equipped trees and time-advanced potentials $\psi(x,t)$ with massive sinks (Sect. 6.4, Constructions 1, 2).

Theorem 7 describes the ballistic annihilation dynamics for the initial velocity field that alternates between ± 1 at epochs of a stationary Poisson point process on $\mathbb{R}$. The respective potential corresponds to the Harris path of a critical binary Galton-Watson tree with i.i.d. exponential edge lengths. This equivalence allows one to use a suit of results available for the exponential Galton-Watson tree to study the

ballistic annihilation; in particular, this connects the ballistic annihilation dynamics with the invariance results of Thms. 2, 3. We use this connection to derive the time-dependent mass distribution of a random sink in an infinite potential (Sect. 6.6, Thm. 9).

The rest of the paper is organized as follows. Section 2 collects necessary results on level set trees. The generalized dynamical pruning is introduced in Sect. 3. The critical binary Galton-Watson trees with i.i.d. exponential edge lengths are introduced and examined in Sect. 4. In particular, the invariance of such trees with respect to the generalized dynamical pruning is established in Sect. 4.3. A continuum 1-D ballistic annihilation model $A + A \to \varnothing$ is introduced in Sect. 5. The dynamics of this model with piece-wise unit slope potential is analyzed in Sect. 6. Sections 6.5, 6.6 examine a unit slope potential with exponential segments durations (Poisson epoch velocity alterations), for a finite and infinite domain, respectively. Section 7 discusses a real tree representation of ballistic annihilation. Section 8 concludes.

2. Trees

This section discusses the basic tools of our analysis – level set tree (Sect. 2.2) and Harris path (Sect. 2.3). We use the framework described in [34] and refer to that work for further details. We start with introducing the relevant spaces of trees.

2.1. Spaces of trees.

Consider the space $\mathcal{T}$ of finite unlabeled rooted reduced trees with no planar embedding. The (combinatorial) distance between a pair of tree vertices is the number of edges in the shortest path between them. A tree is called *rooted* if one of its vertices, denoted by ρ, is selected as the tree root. The existence of root imposes a parent-offspring relation between each pair of adjacent vertices: the one closest to the root is called the *parent*, and the other the *offspring*. The space $\mathcal{T}$ includes the *empty tree* ϕ comprised of a root vertex and no edges. The absence of planar embedding in this context is the absence of order among the offspring of the same parent. The tree root is the only vertex that does not have a parent. We write $\#T$ for the number of non-root vertices, equal to the number of edges, in a tree T. Hence, a finite tree $T = \rho \cup \{v_i, e_i\}_{1 \le i \le \#T}$ is comprised of the root ρ and a collection of non-root vertices v_i, each of which is connected to its unique parent $\mathsf{parent}(v_i)$ by the parental edge e_i, $1 \le i \le \#T$. A tree is called *reduced* if it has no vertices of degree 2, with the root as the only possible exception.

The space of trees from $\mathcal{T}$ with positive edge lengths is denoted by $\mathcal{L}$. The trees in $\mathcal{L}$, also known as *weighted tree* [42], can be considered metric spaces. Specifically, the trees from $\mathcal{L}$ are isometric to one-dimensional connected sets comprised of a finite number of line segments that can share end points. The distance along tree paths is defined according to the Lebesgue measure on the edges.

We write $\mathcal{T}_{\text{plane}}$ and $\mathcal{L}_{\text{plane}}$ for the spaces of trees from $\mathcal{T}$ and $\mathcal{L}$ with planar embedding, respectively. Any tree from $\mathcal{T}$ or $\mathcal{L}$ can be embedded in a plane by selecting an order for the offsprings of the same parent. Unless indicated otherwise, the vertices of an embedded tree are indexed in order of depth-first search, starting from the root.

Sometimes we focus on the combinatorial tree $\textsc{shape}(T)$, which retains the combinatorial structure of $T \in \mathcal{L}$ (or $\mathcal{L}_{\text{plane}}$) while omitting its edge lengths and embedding. Similarly, the combinatorial tree $\textsc{p-shape}(T)$ retains the combinatorial structure of $T \in \mathcal{L}_{\text{plane}}$ and planar embedding, and omits the edge length information. Here $\textsc{shape}$ is a projection from $\mathcal{L}$ or $\mathcal{L}_{\text{plane}}$ to $\mathcal{T}$, and $\textsc{p-shape}$ is a projection from $\mathcal{L}_{\text{plane}}$ to $\mathcal{T}_{\text{plane}}$.

A non-empty rooted tree is called *planted* if its root has degree 1; in this case the only edge connected to the root is called the *stem*. Otherwise the root has degree ≥ 2 and a tree is called *stemless*. We denote by $\mathcal{L}^{\shortmid}$ and $\mathcal{L}^{\vee}$ the subspaces of $\mathcal{L}$ consisting of planted and stemless trees, respectively. Hence $\mathcal{L} = \mathcal{L}^{\shortmid} \cup \mathcal{L}^{\vee}$. Also, we let the empty tree ϕ to be contained in each of the spaces. Therefore, $\mathcal{L}^{\shortmid} \cap \mathcal{L}^{\vee} = \{\phi\}$. Similarly, we write $\mathcal{L}^{\shortmid}_{\text{plane}}$ and $\mathcal{L}^{\vee}_{\text{plane}}$ for the subspaces of $\mathcal{L}_{\text{plane}}$ consisting of planted and stemless trees, respectively. Clearly, $\mathcal{L}_{\text{plane}} = \mathcal{L}^{\shortmid}_{\text{plane}} \cup \mathcal{L}^{\vee}_{\text{plane}}$ and $\mathcal{L}^{\shortmid}_{\text{plane}} \cap \mathcal{L}^{\vee}_{\text{plane}} = \{\phi\}$. Fig. 3 shows examples of a planted and a stemless tree.

For any space $\mathcal{S}$ from the list $\{\mathcal{T}, \mathcal{T}_{\text{plane}}, \mathcal{L}, \mathcal{L}_{\text{plane}}\}$ we write $\mathcal{BS}$ for the respective subspace of *binary* trees, $\mathcal{S}^{\shortmid}$ for the subspace of *planted* trees in $\mathcal{S}$ including ϕ, and $\mathcal{S}^{\vee}$ for the subspace of *stemless* trees in $\mathcal{S}$ including ϕ. We also consider subspaces $\mathcal{BS}^{\shortmid} = \mathcal{S}^{\shortmid} \cap \mathcal{BS}$ of *planted binary* trees and $\mathcal{BS}^{\vee} = \mathcal{S}^{\vee} \cap \mathcal{BS}$ of *stemless binary* trees.

Let $l_T = (l_1, \ldots, l_{\#T})$ with $l_i > 0$ be the vector of edge lengths of a tree $T \in \mathcal{L}$ (or $\mathcal{L}_{\text{plane}}$). The length of a tree T is the sum of the lengths of its edges:

$$\textsc{length}(T) = \sum_{i=1}^{\#T} l_i.$$

Recall that a tree $T \in \mathcal{L}$ can be considered as a metric space with distance $d(\cdot, \cdot)$ induced by the Lebesgue measure along the tree edges

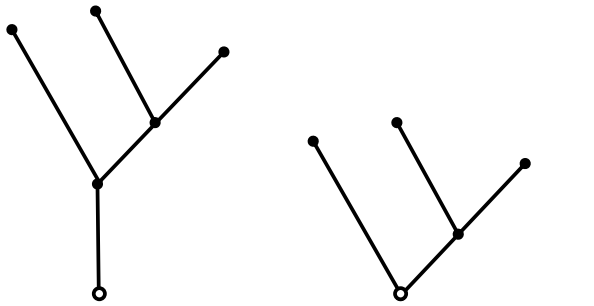

(a) Planted tree, $T \in \mathcal{L}^{|}_{\text{plane}}$ (b) Stemless tree, $T \in \mathcal{L}^{\vee}_{\text{plane}}$

FIGURE 3. Examples of planted (a) and stemless (b) trees.

[34]. The height of a tree T is the maximal distance between the root and a vertex:

$$\text{HEIGHT}(T) = \max_{1 \le i \le \#T} d(v_i, \rho).$$

2.2. **Level set tree.** This section introduces a tree representation of continuous functions, which we call a *level set tree*.

We begin by assuming a finite number of local extrema; this construction is more intuitive and is sufficient for analysis of finite trees from $\mathcal{L}_{\text{plane}}$. Consider a closed interval $I \subset \mathbb{R}$ and function $f(x) \in C(I)$, where $C(I)$ is the space of continuous functions from I to $\mathbb{R}$. Suppose that $f(x)$ has a finite number of distinct local minima. The *level set* $\mathcal{L}_\alpha(f)$ is defined as the pre-image of the function values equal to or above α:

$$\mathcal{L}_\alpha = \mathcal{L}_\alpha(f) = \{x \in I \,:\, f(x) \ge \alpha\}.$$

The level set $\mathcal{L}_\alpha$ for each α is a union of non-overlapping intervals; we write $|\mathcal{L}_\alpha|$ for their number. Notice that $|\mathcal{L}_\alpha| = |\mathcal{L}_\beta|$ as soon as the interval $[\alpha, \beta]$ does not contain a value of local extrema of $f(x)$ and $0 \le |\mathcal{L}_\alpha| \le n$, where n is the total number of the local maxima of $f(x)$ over I.

The *level set tree* $\text{LEVEL}(f) \in \mathcal{L}_{\text{plane}}$ is a tree that describes the structure of the level sets $\mathcal{L}_\alpha$ as a function of threshold α, as illustrated in Fig. 4. Specifically, there are bijections between

- **(i):** the leaves of $\text{LEVEL}(f)$ and the local maxima of $f(x)$;
- **(ii):** the internal (parental) vertices of $\text{LEVEL}(f)$ and the local minima of $f(x)$, excluding possible local minima achieved on the boundary ∂I;

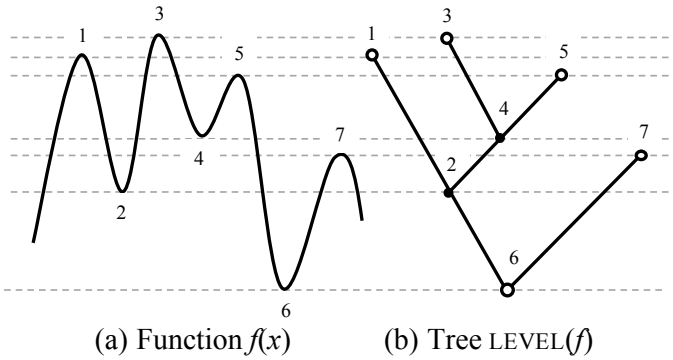

FIGURE 4. Function $f(x)$ (panel a) with a finite number of local extrema and its level set tree $\textsc{level}(f)$ (panel b). In this figure, the distances on a tree (edge lengths) are measured along the y-axis. Dashed horizontal lines and numbers $1, \ldots, 7$ illustrate correspondence between the local extrema of $f(x)$ and vertices of $\textsc{level}(f)$.

(iii): a pair of subtrees of $\textsc{level}(f)$ rooted in the parental vertex that corresponds to a local minima $f(x^*)$ and the adjacent positive excursions (or meanders bounded by ∂I) of $f(x) - f(x^*)$ to the right and left of x^*.

Furthermore, every edge in the tree is assigned a length equal the difference of the values of $f(x)$ at the local extrema that correspond to the vertices adjacent to this edge according to the bijections (i) and (ii) above. The tree root corresponds to the global minimum of $f(x)$ on I. If the minimum is achieved at $x \in I \setminus \partial I$, then the level set tree is stemless, $\textsc{level}(f) \in \mathcal{L}^{\vee}_{\text{plane}}$; this case is shown in Fig. 4. Otherwise, if the minimum is on the boundary ∂I, then the level set tree is planted, $\textsc{level}(f) \in \mathcal{L}^{|}_{\text{plane}}$.

In general, for a function $f(x) \in C(I)$ on a closed interval $I \subset \mathbb{R}$, the level set tree is defined via the framework developed in Aldous [3, 4] and Pitman [42]. Specifically, let $\underline{f}[a,b] := \inf_{x\in[a,b]} f(x)$ for any subinterval $[a,b] \subset I$. We define a *pseudo-metric* on I as [4, 42]

$$d_f(a,b) := \Big(f(a) - \underline{f}[a,b]\Big) + \Big(f(b) - \underline{f}[a,b]\Big), \quad a,b \in I. \tag{1}$$

We write $a \sim_f b$ if $d_f(a,b) = 0$. Here d_f is a metric on the quotient space $I_f \equiv I/\sim_f$. It can be shown [42] that (I_f, d_f) is a tree. This construction is know as the *tree in continuous path* [42, Def. 7.6], [21, Ex. 3.14]. In case of a finite number of local extrema, this construction

coincides with the level-set description given above, that is (I_f, d_f) is isometric to $\textsc{level}(f)$.

2.3. **Harris path.** For any embedded tree $T \in \mathcal{L}_{\text{plane}}$ with edge lengths, the *Harris path* is defined as a piece-wise linear function [27, 42]

$$H_T(t) \,:\, [0, 2 \cdot \textsc{length}(T)] \to \mathbb{R}$$

that equals the distance from the root traveled along the tree T in the depth-first search, as illustrated in Fig. 5. For a tree T with n leaves, the Harris path $H_T(t)$ is a piece-wise linear positive excursion that consists of $2n$ linear segments with alternating slopes ± 1.

2.4. **Reciprocity of Harris path and level set tree.** Consider a function $f(x) \in C(I)$ with a finite number of distinct local minima. By construction, the level set tree $\textsc{level}(f)$ is completely determined by the sequence of the values of local extrema of f, and is not affected by timing of those extrema, as soon as their order is preserved. This means, for instance, that if $g(x)$ is a continuous and monotone increasing function on I, then the trees $\textsc{level}(f)$ and $\textsc{level}(f \circ g)$ are equivalent in $\mathcal{L}_{\text{plane}}$. Hence, without loss of generality we can focus on the level set trees of continuous functions with alternating slopes ± 1. We write $\mathcal{E}^{\text{ex}}$ for the space of all positive piece-wise linear continuous finite *excursions* with alternating slopes ± 1 and a finite number of segments (i.e., a finite number of local extrema). Recall that a continuous function $f(x)$ on a finite interval $[0, a]$ is called an excursion if $f(0) = f(a) = 0$ and $f(x) > 0$ for any $x \in [0, a]$.

The level set tree of an excursion from $\mathcal{E}^{\text{ex}}$ and Harris path are reciprocal to each other as described in the following statement.

Proposition 1 (**Reciprocity of Harris path and level set tree**). *The Harris path $H : \mathcal{L}^{|}_{\text{plane}} \to \mathcal{E}^{\text{ex}}$ and the level set tree $\textsc{level} : \mathcal{E}^{\text{ex}} \to \mathcal{L}^{|}_{\text{plane}}$ are reciprocal to each other. This means that for any $T \in \mathcal{L}^{|}_{\text{plane}}$ we have $\textsc{level}(H_T(t)) \equiv T$, and for any $g(t) \in \mathcal{E}^{\text{ex}}$ we have $H_{\textsc{level}(g)}(t) \equiv g(t)$.*

This statement is illustrated in Fig. 5.

3. Generalized dynamical pruning

This section introduces a general way to prune (cut, erase) a tree from leaves down to the root in an *adaptive, non-anticipating* way, so that the cutting process is completely determined by the parts of the tree that have been cut and is independent of the intact part of the tree.

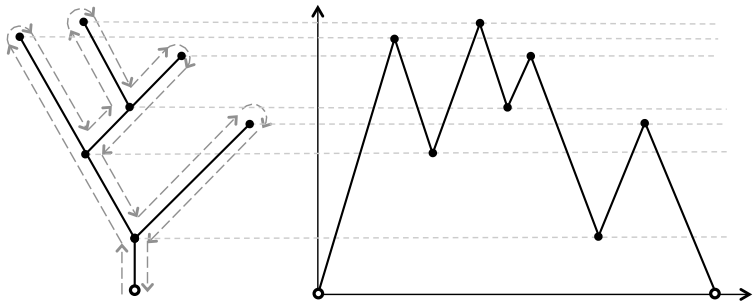

(a) Tree T (b) Harris path H_T

FIGURE 5. (a) Tree T and its depth-first search illustrated by dashed arrows. (b) Harris path $H_T(t)$ for the tree T of panel (a).

3.1. **Definition and examples.** Given a tree $T \in \mathcal{L}$ and a point $x \in T$, let $\Delta_{x,T}$ be the *descendant tree* of x: it is comprised of all points of T descendant to x, including x; see Fig. 6a. Then $\Delta_{x,T}$ is itself a tree in $\mathcal{L}$ with root at x. Let $T_1 = (M_1, d_1)$ and $T_2 = (M_2, d_2)$ be two metric rooted trees, and let ρ_1 denote the root of T_1. A function $f : T_1 \to T_2$ is said to be an *isometry* if $\mathsf{Image}[f] \subseteq \Delta_{f(\rho_1),T_2}$ and for all pairs $x, y \in T_1$,

$$d_2\Big(f(x), f(y)\Big) = d_1(x, y).$$

The tree isometry is illustrated in Fig. 6b. We use the isometry to define a *partial order* in the space $\mathcal{L}$ as follows. We say that T_1 is *less than or equal to* T_2 and write $T_1 \preceq T_2$ if there is an isometry $f : T_1 \to T_2$. The relation $\preceq$ is a partial order as it satisfies the reflexivity, antisymmetry, and transitivity conditions. Moreover, a variety of other properties of this partial order can be observed, including order denseness and semi-continuity.

We say that a function $\varphi : \mathcal{L} \to \mathbb{R}$ is *monotone nondecreasing* with respect to the partial order $\preceq$ if $\varphi(T_1) \le \varphi(T_2)$ whenever $T_1 \preceq T_2$. Consider a monotone nondecreasing function $\varphi : \mathcal{L} \to \mathbb{R}_+$. We define the *generalized dynamical pruning* operator $\mathcal{S}_t(\varphi, T) : \mathcal{L} \to \mathcal{L}$ induced by φ for any $t \ge 0$ as

$$\mathcal{S}_t(\varphi, T) := \rho \cup \Big\{ x \in T \setminus \rho \ : \ \varphi\Big(\Delta_{x,T}\Big) \ge t \Big\}, \tag{2}$$

where ρ denotes the root of tree T. Informally, the operator $\mathcal{S}_t$ cuts all subtrees $\Delta_{x,T}$ for which the value of φ is below threshold t, and always keeps the tree root. Extending the partial order to $\mathcal{L}$ by assuming

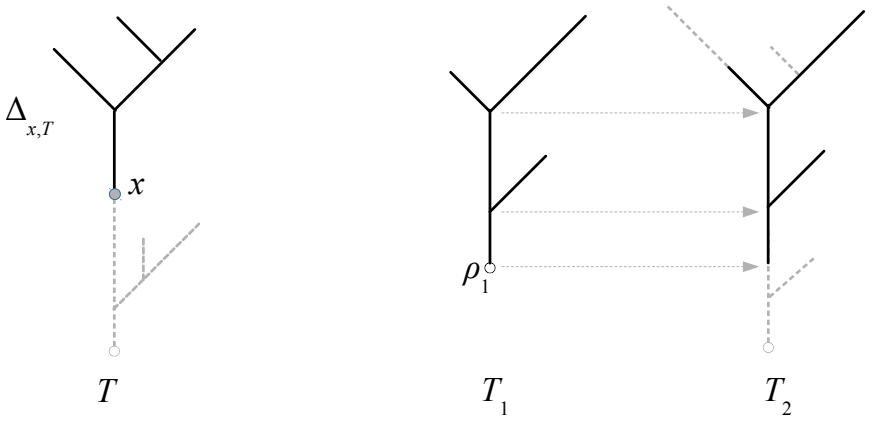

(a) Descendant tree (b) Isometry

FIGURE 6. Descendant subtree and tree isometry: an illustration. (a) Subtree $\Delta_{x,T}$ (solid black lines) descendant to a point x (gray circle) in a tree T (union of dashed gray and soling black lines). (b) Isometry of trees. Tree T_1 (left) is mapped to tree T_2 (right). The image of T_1 within T_2 is shown by black lines, the rest of T_2 is shown by dashed gray lines. Here, tree T_1 is less than tree T_2, $T_1 \preceq T_2$.

$\phi \preceq T$ for all $T \in \mathcal{L}$, we observe for any $T \in \mathcal{L}$ that $S_s(T) \preceq S_t(T)$ whenever $s \geq t$.

The dynamical pruning operator $\mathcal{S}_t$ encompasses and unifies a range of problems, depending on a choice of φ, as we illustrate in the following examples.

Example 1 (Pruning via the tree height). Let the function $\varphi(T)$ equal the height of tree T:

$$\varphi(T) = \text{HEIGHT}(T). \tag{3}$$

In this case the operator $\mathcal{S}_t$ satisfies **continuous semigroup property**:

$$\mathcal{S}_t \circ \mathcal{S}_s = \mathcal{S}_{t+s} \quad \text{for any} \quad t, s \geq 0.$$

It coincides with the continuous pruning (tree erasure) studied in Neveu [38], who established invariance of a critical and sub-critical binary Galton-Watson processes with i.i.d. exponential edge lengths with respect to this operation.

It is readily seen that for a coalescent process [42], the dynamical pruning $\mathcal{S}_t$ of the corresponding coalescent tree with $\varphi(T)$ as in (3) replicates the coalescent process. More specifically, the timing and order of particle mergers is reproduced by the dynamics of the leaves

of $\mathcal{S}_t(\varphi, T)$. See Sect. 6.4, Thm. 5 for a specific version of this statement for the coalescent dynamics of shocks in the continuum ballistic annihilation model.

Example 2 (**Pruning via the Horton-Strahler order).** Let the function $\varphi(T) + 1$ equal the Horton-Strahler order $\mathsf{k}(T)$ of a tree T:

$$\varphi(T) = \mathsf{k}(T) - 1. \tag{4}$$

The Horton-Strahler order [34, 40, 14, 30] is defined via the operation $\mathcal{R}$ of Horton pruning – cutting the leaves with consecutive series reduction (removing degree-2 vertices), as is illustrated in Fig. 7. The pruning induces a contracting map on $\mathcal{BL}_{\text{plane}}$. The trajectory of each tree T under $\mathcal{R}(\cdot)$ is uniquely determined and finite:

$$T \equiv \mathcal{R}^0(T) \to \mathcal{R}^1(T) \to \cdots \to \mathcal{R}^k(T) = \phi, \tag{5}$$

with the empty tree ϕ as the (only) fixed point [33, 34]. The Horton-Strahler order $\mathsf{k}(T)$ of a planted tree from $\mathcal{BL}^{|}_{\text{plane}}$ is the minimal number of prunings necessary to eliminate a tree T. The Horton-Strahler order $\mathsf{k}(T)$ of a stemless tree from $\mathcal{BL}^{\vee}_{\text{plane}}$ is the minimal number of prunings necessary to eliminate a tree T plus one.

With the choice (4) the dynamical pruning operator coincides with the Horton pruning: $\mathcal{S}_t = \mathcal{R}^{\lfloor t \rfloor}$. It is readily seen that $\mathcal{S}_t$ satisfies **discrete semigroup property**:

$$\mathcal{S}_t \circ \mathcal{S}_s = \mathcal{S}_{t+s} \quad \text{for any} \quad t, s \in \mathbb{N}_0.$$

A recent survey of results related to invariance of a tree distribution with respect to Horton pruning is given in [34].

Example 3 (**Pruning via the tree length).** Let the function $\varphi(T)$ equal the total lengths of T:

$$\varphi(T) = \textsc{length}(T). \tag{6}$$

The dynamical pruning by the tree length is illustrated in Fig. 8 for a Y-shaped tree that consists of three edges.

Importantly, in this case $\mathcal{S}_t$ **does not satisfy** the semigroup property. To see this, consider an internal vertex point $x \in T$ (see Fig. 8, where the only internal vertex is marked by a gray ball). Then $\Delta_{x,T}$ consists of point x as its root, the left subtree of length a and the right subtree of length b. Observe that the whole left subtree is pruned away by time a, and the whole right subtree is pruned away by time b. However, since

$$\varphi(\Delta_{x,T}) = \textsc{length}(\Delta_{x,T}) = a + b,$$

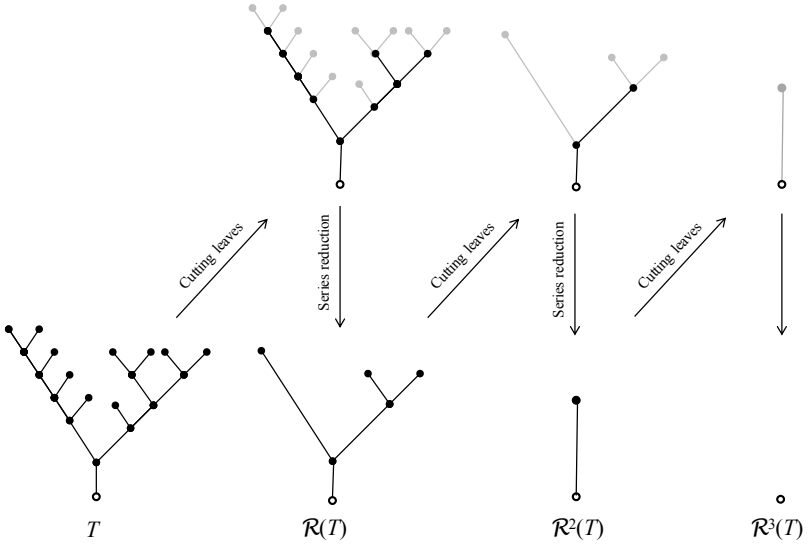

FIGURE 7. Horton pruning and Horton-Strahler ordering: an example. The order of the tree is $\mathsf{k}(T) = 3$, since the tree T is eliminated in three prunings. Each pruning consists of cutting leaves (top row) and consecutive series reduction (bottom row). The pruning trajectory $T \to \mathcal{R}(T) \to \mathcal{R}^2(T) \to \mathcal{R}^3(T) = \phi$ is shown in the bottom row of panels.

the junction point x will not be pruned until time instant $a + b$. Thus, x will be a leaf of $\mathcal{S}_t(\varphi, T)$ for all t such that

$$\max\{a, b\} \le t \le a + b.$$

This situation corresponds to Stage IV in Fig. 8.

The semigroup property in this example can be introduced by considering **mass-equipped trees**. Informally, we replace each pruned subtree τ of T with a point of mass equal to the total length of τ. The massive points contain some of the information lost during the pruning process, which is enough to establish the semigroup property. Specifically, by time a, the pruned away left subtree (Fig. 8, Stage III) turns into a massive point of mass a attached to x on the left side. Similarly, by time b, the pruned away right subtree (Fig. 8, Stage IV) turns into a massive point of mass b attached to x on the right side. For $\max\{a, b\} \le t \le a + b$, this construction keeps track of the quantity $a + b - t$ associated with point x, and when the quantity $a + b - t$ decreases to 0, the two massive points coalesce into one. If at instant t a single massive point seats at a leaf, its mass $m = t$, and the leaf's parental edge is being pruned. If at instant t two massive points (left

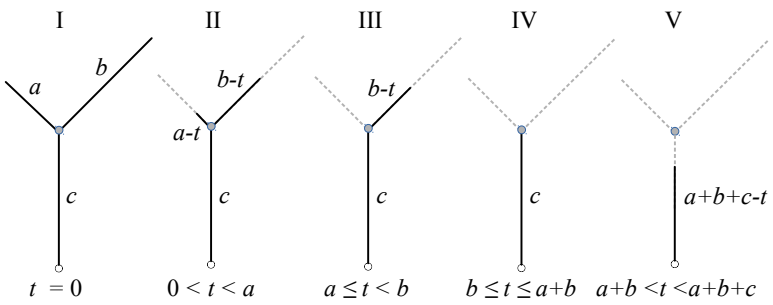

FIGURE 8. Pruning by tree length: an illustration. Figure shows five generic stages in the dynamical pruning of a Y-shaped tree T, with pruning function $\varphi(T) = \text{LENGTH}(T)$. The pruned tree $\mathcal{S}_t$ is shown by solid black lines; the pruned parts of the initial tree are shown by dashed gray lines.
Stage I: Initial tree T consists of three edges, with lengths a, b, c indicated in the panel; without loss of generality we assume $a < b$.
Stage II: For any $t < a$ the pruned tree $\mathcal{S}_t$ has a Y-shaped form with leaf edges truncated by t.
Stage III: For any $a \le t < b$ the pruned tree $\mathcal{S}_t$ consists of a single edge of length $c + b - t$.
Stage IV: For any $b \le t \le a + b$ the pruned tree $\mathcal{S}_t$ consists of a single edge of length c. Notice that during this stage the tree $\mathcal{S}_t$ does not change with t; this loss of memory causes the process to violate the semigroup property.
Stage V: For any $a + b < t < a + b + c$ the pruned tree $\mathcal{S}_t$ consists of a single edge of length $a + b + c - t$.

and right) seat at a leaf, they total mass $m \ge t$, and further pruning of the leaf's parental edge is prevented until the instant $t = m$, when the two massive points coalesce. Keeping track of all such quantities makes $\mathcal{S}_t$ to satisfy the continuous semigroup property. This construction is formally introduced in Sect. 5, which shows that the pruning operator $\mathcal{S}_t$ with the pruning function (6) coincides with the potential dynamics of continuum mechanics formulation of the 1-D ballistic annihilation model $A + A \to \varnothing$.

Example 4 (Pruning via the number of leaves). Let the function $\varphi(T)$ equal the number of leaves in a tree T. This choice is closely related to the mass-conditioned dynamics of an aggregation process. Specifically, consider N singletons (particles with unit mass) that appear in a system at instants $t_n \ge 0$, $1 \le n \le N$. The existing clusters merge into consecutively larger clusters by pair-wise mergers. The cluster mass is additive: a merger of two clusters of masses i and j results

in a cluster of mass $i + j$. We consider a time-oriented tree T that describes this process. The tree T has N leaves and $(N - 1)$ internal vertices. Each leaf corresponds to an initial particle, each internal vertex corresponds to a merger of two clusters, and the edge lengths represent times between the respective mergers. The action of $\mathcal{S}_t$ on such a tree coincides with a conditional state of the process that only considers clusters of mass $\geq t$. A well-studied special case is a coalescent process with a kernel $K(i, j)$, where all particles appear at instant $t = 0$ and each pair of clusters with masses i, j merges with intensity proportional to $K(i, j) = K(j, i)$, independently of all other pairs.

3.2. **Pruning for $\mathbb{R}$-trees.** The generalized dynamical pruning is readily applied to *real trees* (Sect. 7), although this is not the focus of our work. We notice that the total tree length (Example 3) and number of leaves (Example 4) might be undefined (infinite) for an $\mathbb{R}$-tree. We introduce in Sect. 7.3 a *mass* function that can serve as a natural general analog of these and other functions on finite trees. We show (Sect. 6.4, Thm. 6) that pruning by mass is equivalent to the pruning by the total tree lengths in a particular situation of ballistic annihilation model with piece-wise continuous potential with a finite number of segments. Accordingly, our results should be straightforwardly extended to $\mathbb{R}$-trees that appear, for instance, as a description of the continuum ballistic annihilation dynamics for other initial potentials.

3.3. **Relation to other generalizations of pruning.** A pruning operation similar in spirit to the generalized dynamical pruning was considered in a work by Duquesne and Winkel [15] that extended a formalism by Evans [21] and Evans et al. [22]. We notice that the two definitions of pruning, the generalized dynamical pruning of Sect. 3 and that in [15], are principally different, despite their similar appearance. In essence, the work [15] assumes the Borel measurability with respect to the Gromov-Hausdorff metric ([15], Section 2), which implies the semigroup property of the respective pruning ([15], Lemma 3.11). On the contrary, the generalized dynamical pruning defined here may have the semigroup property only under very particular choices of $\varphi(T)$ as in the examples in Sect. 1 and 2. The majority of natural choices of $\varphi(T)$, including the tree length $\varphi(T) = \textsc{length}(T)$ (Example 3) or the number of leaves in a tree (Example 4), do not satisfy the semigroup property, and hence are not covered by the pruning of [15]. The main results of our Sect. 5 refer to the pruning function $\varphi(T) = \textsc{length}(T)$ that does not satisfy the semigroup property, as shown in Sect. 3.

3.4. **Invariance with respect to the generalized dynamical pruning.** Consider a tree $T \in \mathcal{L}_{\text{plane}}$ with edge lengths given by a vector $l_T = (l_1, \dots, l_{\#T})$. The vector l_T can be specified by distribution $\chi(\cdot)$ of a point $x_T = (x_1, \dots, x_{\#T})$ on the standard simplex

$$\Delta^{\#T} = \left\{ x_i : \sum_i^{\#T} x_i = 1, 0 < x_i \le 1 \right\},$$

and conditional distribution $F(\cdot|x_T)$ of the tree length $\textsc{length}(T)$, so that

$$l_T = x_T \cdot \textsc{length}(T).$$

Accordingly, a tree T can be completely specified by its planar shape, a vector of proportional edge lengths, and the total tree length:

$$T = \left\{ \textsc{p-shape}(T), x_T, \textsc{length}(T) \right\}.$$

A measure η on $\mathcal{L}_{\text{plane}}$ is a joint distribution of these three components:

$$\eta(T \in \{\tau, d\bar{x}, d\ell\}) = \mu(\tau) \cdot \chi_\tau(d\bar{x}) \cdot F_{\tau,\bar{x}}(d\ell),$$

where the tree planar shape is specified by

$$\mu(\tau) = \mathsf{Law}\left(\textsc{p-shape}(T) = \tau\right), \quad \tau \in \mathcal{T}_{\text{plane}},$$

the relative edge lengths is specified by

$$\chi_\tau(\bar{x}) = \mathsf{Law}\left(x_T = \bar{x} \,|\, \textsc{p-shape}(T) = \tau\right), \quad \bar{x} \in \Delta^{\#T},$$

and the total tree length is specified by

$$F_{\tau,\bar{x}}(\ell) = \mathsf{Law}\left(\textsc{length}(T) = \ell \,|\, x_T = \bar{x},\ \textsc{p-shape}(T) = \tau\right), \quad \ell \ge 0.$$

Let us fix $t \ge 0$ and a function $\varphi : \mathcal{L}_{\text{plane}} \to \mathbb{R}_+$ that is monotone nondecreasing with respect to the partial order $\preceq$. We denote by $\mathcal{S}_t^{-1}(\varphi, T)$ the preimage of a tree $T \in \mathcal{L}_{\text{plane}}$ under the generalized dynamical pruning:

$$\mathcal{S}_t^{-1}(\varphi, T) = \{\tau \in \mathcal{L}_{\text{plane}} : \mathcal{S}_t(\varphi, \tau) = T\}.$$

Consider the distribution of edge lengths induced by the pruning:

$$\Xi_\tau(\bar{x}) = \mathsf{Law}\left(x_{\tilde{T}} = \bar{x} \,|\, \textsc{p-shape}\left(\tilde{T}\right) = \tau\right)$$

and

$$\Phi_{\tau,\bar{x}}(\ell) = \mathsf{Law}\left(\textsc{length}\left(\tilde{T}\right) = \ell \,|\, x_{\tilde{T}} = \bar{x},\ \textsc{p-shape}\left(\tilde{T}\right) = \tau\right),$$

where the notation $\tilde{T} := \mathcal{S}_t(\varphi, T)$ is used for brevity.

Definition 1 (Generalized prune invariance). *Consider a function*

$$\varphi : \mathcal{L}_{\text{plane}} \to \mathbb{R}_+$$

that is monotone nondecreasing with respect to the partial order $\preceq$. A measure η on $\mathcal{L}_{\text{plane}}$ is called invariant with respect to the generalized dynamical pruning $\mathcal{S}_t(\cdot) = \mathcal{S}_t(\varphi, \cdot)$ (or simply prune invariant) if the following conditions hold for all $t \geq 0$:

(i) *The measure is prune-invariant in shapes. This means that for the pushforward measure $\nu = (\mathcal{S}_t)_*(\mu) = \mu \circ \mathcal{S}_t^{-1}$ we have*

$$\mu(\tau) = \nu(\tau | \tau \neq \phi).$$

(ii) *The measure is prune-invariant in edge lengths. This means that for any combinatorial planar tree $\tau \in \mathcal{T}_{\text{plane}}$*

$$\Xi_\tau(\bar{x}) = \chi_\tau(\bar{x})$$

and there exists a scaling exponent $\zeta \equiv \zeta(\varphi, t) > 0$ such that for any relative edge length vector $\bar{x} \in \Delta^{\#\tau}$ we have

$$\Phi_{\tau,\bar{x}}(\ell) = \zeta^{-1} F_{\tau,\bar{x}}\left(\frac{\ell}{\zeta}\right).$$

This definition unifies multiple invariance properties examined in the literature. For example, the classical work by Neveu [38] establishes prune invariance of critical Galton-Watson trees with i.i.d. exponential edge lengths with respect to tree erasure from leaves at a unit rate, which is equivalent to the generalized dynamical pruning with function $\varphi(T) = \textsc{height}(T)$ (see Example 1). Prune invariance with respect to the Horton pruning (see Example 2 and Fig. 7) has been established by Burd et al. [14] for the combinatorial binary critical Galton-Watson trees with no edge lengths. A comprehensive treatment of tree measures invariant with respect to the Horton pruning is given in [34]. Duquesne and Winkel [15] established prune-invariance of critical Galton-Watson trees with i.i.d. exponential edge lengths with respect to so-called *hereditary property*, which includes the tree erasure of Example 1 and Horton pruning of Example 2. Section 4.3 below establishes prune invariance of critical binary Galton-Watson trees with i.i.d. exponential edge lengths with respect to arbitrary generalized pruning.

4. Exponential critical binary Galton-Watson tree $\mathsf{GW}(\lambda)$

Recall that a (combinatorial) critical binary Galton-Watson tree $T \in \mathcal{T}$ describes a trajectory of the Galton-Watson branching process. The process starts with a single progenitor (tree root) at time $t = 0$. At

each discrete time step every existing population member terminates and produces, equiprobably, either no or two offspring, independently of the other members. We denote the resulting tree distribution on $\mathcal{T}$ by $\mathcal{GW}^{\text{crit}}$.

Definition 2 (**Exponential critical binary Galton-Watson tree**). *We say that a random tree $T \in \mathcal{BL}^{|}_{\text{plane}}$ is an exponential critical binary Galton-Watson tree with parameter $\lambda > 0$, and write $T \stackrel{d}{=} \mathsf{GW}(\lambda)$, if*

(i) *SHAPE(T) is a critical binary Galton-Watson tree $\mathcal{GW}^{\text{crit}}$,*
(ii) *the orientation for every pair of siblings in T is random and symmetric (e.g., in each pair of siblings, a randomly and uniformly selected sibling is assigned a right orientation, and the other is assigned a left orientation),*
(iii) *given SHAPE(T), the edges of T are sampled as independent exponential random variables with parameter λ, i.e., with density*

$$\phi_\lambda(x) = \lambda e^{-\lambda x} \mathbf{1}_{\{x \geq 0\}}. \tag{7}$$

The following result is well-known.

Theorem 1. [42, Lemma 7.3],[36, 39] *Consider a random excursion $X_t \in \mathcal{E}^{\text{ex}}$. The level set tree LEVEL(X_t) is an exponential critical binary Galton-Watson tree $\mathsf{GW}(\lambda)$ if and only if the rises and falls of X_t, excluding the last fall, are distributed as independent exponential random variables with parameter $\lambda/2$.*

Consider a random walk $\{X_k\}_{k\in\mathbb{Z}}$ with a homogeneous transition kernel $p(x, y) \equiv p(x - y)$, for any $x, y \in \mathbb{R}$, given by a mixture of exponential jumps (Laplace distribution):

$$p(x) = \frac{\phi_\lambda(x) + \phi_\lambda(-x)}{2} = \frac{\lambda}{2} e^{-\lambda|x|}, \quad -\infty < x < \infty. \tag{8}$$

This process is called a *symmetric exponential random walk* with parameter λ. Each symmetric exponential random walk with parameter λ corresponds to a piece-wise linear continuous function $\{X_t\}_{t\in\mathbb{R}}$ with slopes ± 1 whose alternating rises and falls, taken from $\{X_k\}_{k\in\mathbb{Z}}$, have independent exponential lengths with parameter $\lambda/2$. Specifically, consider a piece-wise linear function that interpolates the local extrema of X_k; then transform the time in such a way that the slopes of the linear interpolation are ± 1. There is one-to-one correspondence between the infinite sequences of the values of local extrema of $\{X_t\}_{t\in\mathbb{R}}$ and $\{X_k\}_{k\in\mathbb{Z}}$. We refer to such a function as a symmetric exponential random walk with parameter $\lambda/2$ on $\mathbb{R}$.

Corollary 1. *The Harris path $H_{\mathsf{GW}(\lambda)}$ of an exponential critical binary Galton-Watson tree with parameter λ is an excursion of a symmetric exponential random walk $\{X_t\}_{t\in\mathbb{R}}$ with parameter $\lambda/2$.*

The main result of this work is Thm. 2 of Sect. 4.3 that establishes invariance of exponential critical binary Galton-Watson tree $\mathsf{GW}(\lambda)$ with respect to an arbitrary generalized dynamical pruning. We begin by finding the distributions of the length and height of this tree; these two distributions are used in Thm. 3 that specifies the scaling of edges in $\mathsf{GW}(\lambda)$ after selected prunings.

4.1. **Length of a random tree $\mathsf{GW}(\lambda)$.** Recall the modified Bessel functions of the first kind

$$I_\nu(z) = \sum_{n=0}^{\infty} \frac{\left(\frac{z}{2}\right)^{2n+\nu}}{\Gamma(n+1+\nu)\, n!}.$$

Lemma 1. *Suppose $T \stackrel{d}{=} \mathsf{GW}(\lambda)$ is an exponential critical binary Galton-Watson tree with parameter λ. The total length of the tree T has the probability density function*

$$\ell(x) = \frac{1}{x} e^{-\lambda x} I_1\Big(\lambda x\Big), \quad x > 0. \tag{9}$$

Proof. The number of different combinatorial shapes of a planar binary tree with $n+1$ leaves, and therefore $2n+1$ edges, is given by the *Catalan number* $C_n = \frac{1}{n+1}\binom{2n}{n} = \frac{(2n)!}{(n+1)!n!}$. The total length of $2n+1$ edges is a gamma random variable with parameters λ and $2n+1$ and density function

$$\gamma_{\lambda,2n+1}(x) = \frac{\lambda^{2n+1} x^{2n} e^{-\lambda x}}{\Gamma(2n+1)}, \quad x > 0.$$

Hence, the total length of the tree T has the probability density function

$$\begin{aligned} \ell(x) &= \sum_{n=0}^{\infty} \frac{C_n}{2^{2n+1}} \cdot \frac{\lambda^{2n+1} x^{2n} e^{-\lambda x}}{(2n)!} = \sum_{n=0}^{\infty} \frac{\lambda^{2n+1} x^{2n} e^{-\lambda x}}{2^{2n+1}(n+1)!n!} \\ &= \frac{1}{x} e^{-\lambda x} \sum_{n=0}^{\infty} \frac{\left(\frac{\lambda x}{2}\right)^{2n+1}}{\Gamma(n+2)\, n!} = \frac{1}{x} e^{-\lambda x} I_1\Big(\lambda x\Big). \end{aligned} \tag{10}$$

□ □

Next, we compute the Laplace transform of $\ell(x)$. By the summation formula in (10),

$$\begin{aligned}\mathcal{L}\ell(s) &= \int_0^\infty \sum_{n=0}^\infty \frac{C_n}{2^{2n+1}} \cdot \frac{\lambda^{2n+1} x^{2n} e^{-(\lambda+s)x}}{(2n)!}\, dx \\ &= \sum_{n=0}^\infty \frac{C_n}{2^{2n+1}} \cdot \left(\frac{\lambda}{\lambda+s}\right)^{2n+1} \int_0^\infty \frac{(\lambda+s)^{2n+1} x^{2n} e^{-(\lambda+s)x}}{(2n)!}\, dx \\ &= \sum_{n=0}^\infty \frac{C_n}{2^{2n+1}} \cdot \left(\frac{\lambda}{\lambda+s}\right)^{2n+1} = Z \cdot c(Z^2),\end{aligned}$$

where we let $Z = \frac{\lambda}{2(\lambda+s)}$, and the characteristic function of Catalan numbers

$$c(z) = \sum_{n=0}^\infty C_n z^n = \frac{2}{1+\sqrt{1-4z}}$$

is well known. Therefore

$$\mathcal{L}\ell(s) = Z \cdot c(Z^2) = \frac{\lambda}{\lambda + s + \sqrt{(\lambda+s)^2 - \lambda^2}}. \tag{11}$$

Note that the Laplace transform $\mathcal{L}\ell(s)$ could be derived from the total probability formula

$$\ell(x) = \frac{1}{2}\phi_\lambda(x) + \frac{1}{2}\phi_\lambda * \ell * \ell(x), \tag{12}$$

where $\phi_\lambda(x)$ is the exponential p.d.f. (7). Thus, $\mathcal{L}\ell(s)$ solves

$$\mathcal{L}\ell(s) = \frac{1}{2}\frac{\lambda}{\lambda+s}\Big(1 + \big(\mathcal{L}\ell(s)\big)^2\Big). \tag{13}$$

Corollary 2. *The probability density function $f(x)$ of the length of an excursion in an exponential symmetric random walk with parameter λ is given by*

$$f(x) = \frac{1}{2}\ell(x/2). \tag{14}$$

Proof. Observe that the excursion has twice the length of a tree $\mathsf{GW}(\lambda)$. □ □

4.2. Height of a random tree $\mathsf{GW}(\lambda)$.

Lemma 2. *Suppose $T \overset{d}{\sim} \mathsf{GW}(\lambda)$ is an exponential critical binary Galton-Watson tree with parameter λ. Then, the height $\textsc{height}(T)$ of the tree T has the cumulative distribution function*

$$\mathsf{H}(x) = \frac{\lambda x}{\lambda x + 2}, \quad x > 0. \tag{15}$$

Proof. The proof is based on duality between trees and positive real excursions. Specifically, Thm. 1 establishes equivalence between the level set tree of a positive excursion of an exponential random walk (Def. 4) and an exponential critical binary Galton-Watson tree $\mathsf{GW}(\lambda)$. This implies, in particular, that for a tree $T \overset{d}{\sim} \mathsf{GW}(\lambda)$ the $\textsc{height}(T)$ has the same distribution as the height of a positive excursion of an exponential random walk Y_k with $Y_0 = 0$ and independent increments $Y_{k+1} - Y_k$ distributed according to the Laplace density function $\frac{\phi_\lambda(x)+\phi_\lambda(-x)}{2} = \frac{\lambda}{2} e^{-\lambda|x|}$, with $\phi_\lambda(x)$ defined in (7).

Notice that Y_k is a martingale. We condition on $Y_1 > 0$, and consider an excursion $Y_0, Y_1, \ldots, Y_{\tau_-}$ with $\tau_- = \min\{k > 1 \ : \ Y_k \le 0\}$ denoting the termination step of the excursion. For $x > 0$, we write

$$p_x = 1 - \mathsf{H}(x) = \mathsf{P}\left(\max_{j:\ 0<j<\tau_-} Y_j > x \ \middle|\ Y_1 > 0 \right)$$

for the probability that the height of the excursion exceeds x. The problem of finding p_x is solved using the Optional Stopping Theorem. Let

$$\tau_x = \min\{k > 0 \ : \ Y_k \ge x\} \qquad \text{and} \qquad \tau := \tau_x \wedge \tau_-.$$

Observe that

$$p_x = \mathsf{P}(\tau = \tau_x \mid Y_1 > 0).$$

For a fixed $y \in (0, x)$, by the Optional Stopping Theorem, we have

$$\begin{aligned}
y &= \mathsf{E}[Y_\tau \mid Y_1 = y] \\
&= \mathsf{E}[Y_\tau \mid \tau = \tau_-, Y_1 = y]\, \mathsf{P}(\tau = \tau_- \mid Y_1 = y) \\
&\qquad + \mathsf{E}[Y_\tau \mid \tau = \tau_x, Y_1 = y]\, \mathsf{P}(\tau = \tau_x \mid Y_1 = y) \\
&= \mathsf{E}[Y_\tau \mid Y_\tau \le 0, Y_1 = y] \mathsf{P}\left(\tau = \tau_- \mid Y_1 = y\right) \\
&\qquad + \mathsf{E}[Y_\tau \mid Y_\tau \ge x, Y_1 = y]\, \mathsf{P}(\tau = \tau_x \mid Y_1 = y) \\
&= -\frac{1}{\lambda} \mathsf{P}(\tau = \tau_- \mid Y_1 = y) + \left(x + \frac{1}{\lambda}\right) \mathsf{P}(\tau = \tau_x \mid Y_1 = y) \\
&= \left(x + \frac{2}{\lambda}\right) \mathsf{P}(\tau = \tau_x \mid Y_1 = y) - \frac{1}{\lambda}.
\end{aligned}$$

Hence,

$$\mathsf{P}(\tau = \tau_x \mid Y_1 = y) = \frac{y + \frac{1}{\lambda}}{x + \frac{2}{\lambda}}.$$

Thus,

$$\begin{aligned}\mathsf{P}\Big(\tau=\tau_x, 0<Y_1<x \mid Y_1>0\Big) &= \int_0^x \mathsf{P}(\tau=\tau_x \mid Y_1=y)\ \lambda e^{-\lambda y}dy \\ &= \int_0^x \frac{y+\frac{1}{\lambda}}{x+\frac{2}{\lambda}}\ \lambda e^{-\lambda y}dy \\ &= \frac{2}{\lambda x+2}-e^{-\lambda x},\end{aligned}$$

and therefore,

$$\begin{aligned}p_x &= \mathsf{P}\left(\max_{j:\ 0<j<K} Y_j > x \mid Y_1>0\right) \\ &= \mathsf{P}\Big(\tau=\tau_x, 0<Y_1<x \mid Y_1>0\Big)+\mathsf{P}\Big(\tau=\tau_x, Y_1\geq x \mid Y_1>0\Big) \\ &= \frac{2}{\lambda x+2}-e^{-\lambda x}+\mathsf{P}\Big(Y_1\geq x \mid Y_1>0\Big)=\frac{2}{\lambda x+2}.\end{aligned}$$

Hence,

$$\mathsf{H}(x)=1-p_x=\frac{\lambda x}{\lambda x+2}.$$

□ □

4.3. **Prune invariance of $\mathsf{GW}(\lambda)$.** This section establishes prune invariance of exponential Galton-Watson trees with respect to arbitrary generalized pruning.

Theorem 2. *Let $T \overset{d}{\sim} \mathsf{GW}(\lambda)$, $T \in \mathcal{BL}^{|}_{\text{plane}}$, be an exponential critical binary Galton-Watson tree with parameter $\lambda > 0$. Then, for any monotone nondecreasing function $\varphi : \mathcal{BL}^{|}_{\text{plane}} \to \mathbb{R}_+$ and any $\Delta > 0$ we have*

$$T^{\Delta} := \{\mathcal{S}_{\Delta}(\varphi, T) | \mathcal{S}_{\Delta}(\varphi, T) \neq \phi\} \overset{d}{\sim} \mathsf{GW}(\lambda p_{\Delta}(\lambda, \varphi)),$$

where $p_{\Delta}(\lambda, \varphi) = \mathsf{P}(\mathcal{S}_{\Delta}(\varphi, T) \neq \phi)$. That is, the pruned tree T^{Δ} conditioned on surviving is an exponential critical binary Galton-Watson tree with parameter

$$\mathcal{E}_{\Delta}(\lambda, \varphi) = \lambda p_{\Delta}(\lambda, \varphi).$$

Proof. Let X denote the length of the stem (edge adjacent to the root) in T, and Y denote the length of the stem in T^{Δ}. Let x be the nearest descendent vertex (a junction or a leaf) to the root in T. Then X, which is an exponential random variable with parameter λ, represents the distance from the root of T to x. Let $\mathsf{deg}_T(x)$ denote the degree of

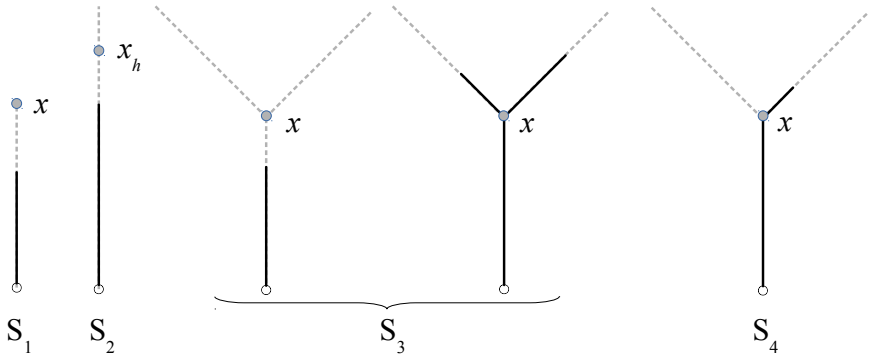

FIGURE 9. Sub-events used in the proof of Thm. 2. Gray dashed line shows (a part of) initial tree T. Solid black line shows (a part of) pruned tree T^{Δ}. We denote by x_h a point in T located at distance h from the root, if it exists.

x in tree T and $\mathsf{deg}_{T^{\Delta}}(x)$ denote the degree of x in tree T^{Δ}. If $T^{\Delta} = \phi$, then $Y = 0$. Let

$$F(h) = \mathsf{P}(Y \le h \mid \mathcal{S}_{\Delta}(\varphi, T) \neq \phi).$$

Let x_h denote a point in T located at distance h from the root, if such exists. If $X \ge h$, the choice of x_h is unique. The event $\{Y \le h\}$ is partitioned into the following non-overlapping sub-events $\mathrm{S}_1, \ldots, \mathrm{S}_4$ illustrated in Fig. 9:

(S_1) The event $\mathrm{S}_1 = \Big\{\mathsf{deg}_T(x) = 1 \text{ and } X \le h\Big\}$ has probability

$$\mathsf{P}(\mathrm{S}_1) = \frac{1}{2}(1 - e^{-\lambda h})$$

as $\mathsf{P}\Big(\mathsf{deg}_T(x) = 1\Big) = \frac{1}{2}$ and $\mathsf{P}(X \le h) = 1 - e^{-\lambda h}$.

(S_2) Denote $p_{\Delta} = p_{\Delta}(\lambda, \varphi)$. The event

$\mathrm{S}_2 = \Big\{X > h$ and all points of T descendant to x_h do not belong to $T^{\Delta}\Big\}$

has probability

$$\mathsf{P}(\mathrm{S}_2) = e^{-\lambda h}(1 - p_{\Delta})$$

as $\mathsf{P}(X > h) = e^{-\lambda h}$ and

$$\mathsf{P}\Big(\text{all points of } T \text{ descendant to } x_h \text{ do not belong to } T^{\Delta} \,|\, X > h\Big)$$
$$= \mathsf{P}\Big(\mathcal{S}_{\Delta}(\varphi, \Delta_{x_h,T}) = \phi \,\Big|\, X > h\Big) = \mathsf{P}(\mathcal{S}_{\Delta}(\varphi, T) = \phi) = 1 - p_{\Delta}.$$

(S_3) The event $\mathrm{S}_3 = \Big\{X \le h$ and $\mathsf{deg}_T(x) = 3$ and either both subtrees of T descending from x are pruned away completely (not

intersecting T^Δ) or $\{x \in T^\Delta,\ \mathsf{deg}_{T^\Delta}(x) = 3\}\Big\}$ has probability

$$\mathsf{P}(\mathrm{S}_3) = \frac{1}{2}(1 - e^{-\lambda h})\Big((1-p_\Delta)^2 + p_\Delta^2\Big)$$

as $\mathsf{P}\Big(\mathsf{deg}_T(x) = 3\Big) = \frac{1}{2}$, $\mathsf{P}(X \le h) = 1 - e^{-\lambda h}$,

$$\mathsf{P}\Big(\text{both subtrees of } T \text{ descending from } x \text{ are pruned away} \,\Big|\, \mathsf{deg}_T(x) = 3\Big) = (1-p_\Delta)^2,$$

and

$$\mathsf{P}\Big(\text{both subtrees of } T \text{ descending from } x \text{ survive pruning} \,\Big|\, \mathsf{deg}_T(x) = 3\Big) = p_\Delta^2.$$

(S_4) The event

$$\mathrm{S}_4 = \{X \le h,\, \mathsf{deg}_T(x) = 3\} \cap \{x \in T^\Delta,\ \mathsf{deg}_{T^\Delta}(x) = 2\} \cap \{Y \le h\}$$

has probability[1]

$$\mathsf{P}(\mathrm{S}_4) = \frac{1}{2}\int_0^h \lambda e^{-\lambda t}\cdot 2p_\Delta(1-p_\Delta)\cdot F(h-t)\,dt = p_\Delta(1-p_\Delta)\int_0^\infty \lambda e^{-\lambda t}F(h-t)\,dt$$

as $\mathsf{P}\Big(\mathsf{deg}_T(x) = 3\Big) = \frac{1}{2}$, $\mathsf{P}\Big(\mathsf{deg}_{T^\Delta}(x) = 2 \,\Big|\, \mathsf{deg}_T(x) = 3\Big) = 2p_\Delta(1-p_\Delta)$, and

$$\mathsf{P}\Big(X \le h, Y \le h \,\Big|\, \mathsf{deg}_T(x) = 3,\ x \in T^\Delta,\ \mathsf{deg}_{T^\Delta}(x) = 2\Big) = \int_0^h \lambda e^{-\lambda t}F(h-t)\,dt.$$

Using the probabilities $\mathsf{P}(\mathrm{S}_1)$, $\mathsf{P}(\mathrm{S}_2)$, $\mathsf{P}(\mathrm{S}_3)$, and $\mathsf{P}(\mathrm{S}_4)$ as obtained above, we have two alternative representations for the probability $\mathsf{P}(Y \le h)$:
First,

$$\mathsf{P}(Y \le h) = (1-p_\Delta) + p_\Delta F(h),$$

[1]Here, $\mathsf{deg}_{T^\Delta}(x) = 2$ means x is neither a junction nor a leaf in T^Δ.

and second,

$$\begin{aligned}\mathsf{P}(Y \le h) =& \mathsf{P}(\mathrm{S}_1) + \mathsf{P}(\mathrm{S}_2) + \mathsf{P}(\mathrm{S}_3) + \mathsf{P}(\mathrm{S}_4)\\ =& \frac{1}{2}(1 - e^{-\lambda h}) + e^{-\lambda h}(1 - p_\Delta)\\ &+ \frac{1}{2}(1 - e^{-\lambda h})\Big((1 - p_\Delta)^2 + p_\Delta^2\Big)\\ &+ p_\Delta(1 - p_\Delta) \int_0^\infty \lambda e^{-\lambda t} F(h - t)\, dt.\end{aligned}$$

Equating the two expressions of $\mathsf{P}(Y \le h)$ and simplifying, we obtain

$$(1-p_\Delta)+p_\Delta F(h) = (1-p_\Delta+p_\Delta^2)-e^{-\lambda h}p_\Delta+p_\Delta(1-p_\Delta)\int_0^\infty \lambda e^{-\lambda t}F(h-t)\, dt.$$

Differentiating the above equality we obtain the following equation for the p.d.f. $f(t) = \frac{d}{dt}F(t)$ of Y:

$$f(h) = p_\Delta\, \phi_\lambda(h) + (1 - p_\Delta)\, \phi_\lambda * f(h),$$

where as before ϕ_λ denotes the exponential density with parameter λ as in (7). Applying integral transformation on both sides of the equation, we obtain the characteristic function $\widehat{f}(s) = \mathsf{E}\Big[e^{isY}\Big]$ of Y,

$$\widehat{f}(s) = \frac{\lambda p_\Delta}{\lambda p_\Delta - is} = \widehat{\phi}_{\lambda p_\Delta}(s).$$

Thus, we conclude that Y is an exponential random variable with parameter λp_Δ.

Next, let y be the descendent vertex (a junction or a leaf) to the root in T^Δ. If $T^\Delta = \phi$, let y denote the root. Let

$$q = \mathsf{P}\Big(\mathsf{deg}_{T^\Delta}(y) = 3 \;\Big|\; S_\Delta(\varphi, T) \neq \phi\Big).$$

As T^Δ is a subset of the metric space T, y is also a point in T which may or may not match x. Then, $\mathsf{P}\Big(\mathsf{deg}_{T^\Delta}(y) = 3 \;\Big|\; y \neq x,\ T^\Delta \neq \phi\Big) = q$ as in the event conditioned upon, y is the descendent vertex to x in T^Δ. Also,

$$\mathsf{P}\Big(y = x \mid \mathsf{deg}_T(x) = 3\Big) = \mathsf{P}\Big(\mathsf{deg}_{T^\Delta}(x) = 3 \mid \mathsf{deg}_T(x) = 3\Big) = p_\Delta^2$$

and

$$\mathsf{P}\Big(y \neq x \mid \mathsf{deg}_T(x) = 3\Big) = \mathsf{P}\Big(\mathsf{deg}_{T^\Delta}(x) = 2 \mid \mathsf{deg}_T(x) = 3\Big) = 2p_\Delta(1-p_\Delta).$$

Therefore, since $\{\mathsf{deg}_{T^\Delta}(y)=3\}$ can be written as the following union of disjoint events,

$$\{\mathsf{deg}_{T^\Delta}(y)=3\} = \{\mathsf{deg}_{T^\Delta}(x)=3,\ y=x\}\cup\{\mathsf{deg}_T(x)=3,\ y\neq x,\ \mathsf{deg}_{T^\Delta}(y)=3\},$$

$$\begin{aligned} q\cdot p_\Delta = \mathsf{P}(\mathsf{deg}_{T^\Delta}(y)=3) =& \mathsf{P}(\mathsf{deg}_T(x)=3)\Big[\mathsf{P}\Big(\mathsf{deg}_{T^\Delta}(x)=3 \mid \mathsf{deg}_T(x)=3\Big) \\ &+ q\,\mathsf{P}\Big(\mathsf{deg}_{T^\Delta}(x)=2 \mid \mathsf{deg}_T(x)=3\Big)\Big] \\ =& \frac{1}{2}\Big[p_\Delta^2 + 2p_\Delta(1-p_\Delta)q\Big] \end{aligned}$$

implying

$$q = \frac{1}{2}p_\Delta + (1-p_\Delta)q,$$

which in turn yields $q=\frac{1}{2}$.

Finally, if $Y\geq h$, let x_h denote the unique point of T located at distance h from the root that survived the pruning. Letting $T^\Delta_{x_h} := \mathcal{S}_\Delta(\varphi, \Delta_{x_h,T})$, we have

$$\Big(T^\Delta_{x_h}\,\Big|\,Y>h\Big) \stackrel{d}{=} \Big(T^\Delta\,\Big|\,S_\Delta(\varphi,T)\neq\phi\Big).$$

Hence, conditioned on $S_\Delta(\varphi,T)\neq\phi$, the events $\Big\{\mathsf{deg}_{T^\Delta}(y)=3\Big\}$ and $\Big\{Y>h\Big\}$ are independent.

We saw that conditioning on $\mathcal{S}_\Delta(\varphi,T)\neq\phi$, the pruned tree T^Δ has the stem length distributed exponentially with parameter λp_Δ. Next, independently of the stem length Y, we have the pruned tree T^Δ branching at y (the stem end point farthest from the root), with probability $q=\frac{1}{2}$, into two independent subtrees, each distributed[2] as $\{T^\Delta \mid T^\Delta\neq\phi\}$. Thus, we recursively obtain that T^Δ is a critical binary Galton-Watson tree with i.i.d. exponential edge length with parameter λp_Δ. □ □

Next, we find an exact form of the survival probability $p_\Delta(\lambda,\varphi)$ for three particular choices of φ, thus obtaining $\mathcal{E}_\Delta(\lambda,\varphi)$.

Theorem 3. *In the settings of Theorem 2, we have*

(a): *If $\varphi(T)$ equals the total length of T ($\varphi = \textsc{length}(T)$), then*

$$\mathcal{E}_\Delta(\lambda,\varphi) = \lambda e^{-\lambda\Delta}\Big[I_0(\lambda\Delta)+I_1(\lambda\Delta)\Big].$$

(b): *If $\varphi(T)$ equals the height of T ($\varphi = \textsc{height}(T)$), then*

$$\mathcal{E}_\Delta(\lambda,\varphi) = \frac{2\lambda}{\lambda\Delta+2}.$$

[2]Here, y is also a junction vertex in T of which it is only known that both of its descendent subtrees survived pruning (were not completely erased).

(c): *If $\varphi(T)+1$ equals the Horton-Strahler order of the tree T, then*

$$\mathcal{E}_\Delta(\lambda,\varphi) = \lambda 2^{-\lfloor \Delta \rfloor},$$

where $\lfloor \Delta \rfloor$ denotes the maximal integer $\leq \Delta$.

Proof. **Part (a).** Suppose $T \overset{d}{\sim} \mathsf{GW}(\lambda)$, and let $\ell(x)$ once again denote the p.d.f. of the total length $\textsc{length}(T)$. Then, by Lemma 1,

$$\begin{aligned} p_\Delta =& 1 - \int_0^\Delta \ell(x)\,dx = 1 - \int_0^{\lambda\Delta} \frac{1}{x} e^{-x} I_1\Big(x\Big)\,dx \\ &= e^{-\lambda\Delta}\Big[I_0(\lambda\Delta) + I_1(\lambda\Delta)\Big], \end{aligned} \tag{16}$$

where for the last equality we used formula 11.3.14 in [2].

Part (b). Suppose $T \overset{d}{\sim} \mathsf{GW}(\lambda)$. Let $\mathsf{H}(x)$ once again denote the cumulative distribution function of the height $\textsc{height}(T)$. Then by Lemma 2, for any $\Delta > 0$,

$$p_\Delta = 1 - \mathsf{H}(\Delta) = \frac{2}{\lambda\Delta + 2}.$$

Part (c). Follows from [33, Corollary 1]. □ □

Remark 1. Let $\mathcal{E}_\Delta(\lambda,\varphi) = \frac{2\lambda}{\lambda\Delta+2}$ as in Theorem 3(b). Here $\mathcal{E}_0(\lambda,\varphi) = \lambda$ and $\mathcal{E}_\Delta(\lambda,\varphi)$ is a linear-fractional transformation associated with matrix

$$\mathcal{A}_\Delta = \begin{pmatrix} 1 & 0 \\ \frac{\Delta}{2} & 1 \end{pmatrix}.$$

Since $\mathcal{A}_\Delta$ form a subgroup in $SL_2(\mathbb{R})$, the transformations $\{\mathcal{E}_\Delta\}_{\Delta\geq 0}$ satisfy the semigroup property

$$\mathcal{E}_{\Delta_1}\mathcal{E}_{\Delta_2} = \mathcal{E}_{\Delta_1+\Delta_2}$$

for any pair $\Delta_1, \Delta_2 \geq 0$.

We notice also that the operator $\mathcal{E}_\Delta(\lambda,\varphi)$ in part (c) of Theorem 3 satisfies only the discrete semigroup property for nonnegative integer times. Finally, one can check that $\mathcal{E}_\Delta(\lambda,\varphi)$ in part (a) does not satisfy the semigroup property.

5. Continuum 1-D ballistic annihilation

As an illuminating application of the generalized dynamical pruning (Sect. 3) and its invariance properties (Sect. 3.4), we consider the dynamics of particles governed by 1-D ballistic annihilation model, traditionally denoted $A+A \to \varnothing$ [18]. This model describes the dynamics of particles on a real line: a particle with Lagrangian coordinate x moves with a constant velocity $v(x)$ until it collides with another particle, at which moment both particles annihilate, hence the model notation. The annihilation dynamics appears in chemical kinetics and bimolecular reactions and has received attention in physics and probability literature [18, 7, 9, 41, 17, 8, 19, 13, 35, 44]. We introduce here a continuum mechanics formulation of ballistic annihilation. The dynamics of a ballistic annihilation model with two coalescing sinks is illustrated in Fig. 1.

Sect. 5.1 introduces the continuum annihilation model and describes the emergence of sinks (shocks). The model initial conditions are given by a particle velocity distribution and particle density on $\mathbb{R}$. Subsequently, we only consider a constant density and initial velocity distribution with alternating values ± 1, or, equivalently, initial piece-wise linear potential $\psi(x,0)$ with alternating slopes ± 1 (Fig. 2). Section 6 discusses a construction of the graphical embedding of the shock wave tree into the phase space $(x, \psi(x,t))$ and space-time domain (x,t). Theorems 5, 6 in Sect. 6.4 establish equivalence of the ballistic annihilation dynamics to the generalized dynamical pruning of a (mass-equipped) shock wave tree. Sections 6.5,6.6 illustrate how the pruning interpretation of annihilation dynamics facilitates analytical treatment of the model. Specifically, we give a complete description of the time-advanced potential function $\psi(x,t)$ at any instant $t > 0$ for the initial potential in a form of exponential excursion (Thm. 7), and describe the temporal dynamics of a random sink (Thms. 8,9).

5.1. Sinks, massive particles, shock waves.

We consider a Lebesgue measurable initial density $g(x,0) = g(x) \geq 0$ of particles on an interval $[a,b] \subset \mathbb{R}$. The initial particle velocities are given by $v(x,0) = v(x)$. Prior to collision and subsequent annihilation, a particle located at x_0 at time $t = 0$ moves according to its initial velocity, so its coordinate $x(t)$ changes as

$$x(t) = x_0 + tv(x_0). \tag{17}$$

When the particle collides with another particle, it annihilates. Accordingly, two particles with initial coordinates and velocities (x_-, v_-) and (x_+, v_+) collide and annihilate at time t when they meet at the

same new position,

$$x_- + tv_- = x_+ + tv_+,$$

given that neither of the particles annihilated prior to t. In this case, the annihilation time is given by

$$t = -\frac{x_+ - x_-}{v_+ - v_-}. \tag{18}$$

Let $g(x,t)$ and $v(x,t)$ be the Eulerian specification of the particle density and velocity field, respectively, at coordinate x and time instant t, with a convention that $g(x,t) = 0 \Rightarrow v(x,t) = 0$. We define the corresponding *potential function*

$$\psi(x,t) = -\int_a^x v(y,t)dy, \quad x \in [a,b], t \geq 0,$$

so that $v(x,t) = -\partial_x \psi(x,t)$. Let $\psi(x,0) = \Psi_0(x)$ be the initial potential.

We call a point $\sigma(t)$ *sink* (or *shock*), if there exist two particles that annihilate at coordinate $\sigma(t)$ at time t. Suppose $v(x) \in C^1(\mathbb{R})$. The equation (18) implies that appearance of a sink is associated with a negative local minima of $v'(x^*)$; we call such points *sink sources*. Specifically, if x^* is a sink source, then a sink will appear at *breaking time* $t^* = -1/v'(x^*)$ at the location given by

$$\sigma(t^*) = x^* + t^* v(x^*) = x^* - \frac{v(x^*)}{v'(x^*)},$$

provided there exists a punctured neighborhood

$$N_\delta(x^*) = \{x : \ 0 < |x - x^*| < \delta\} \subseteq [a,b]$$

such that none of the particles with the initial coordinates in $N_\delta(x^*)$ is annihilated before time t^*.

Sinks, which originate at sink sources, can move and coalesce (see Fig. 1). We impose the conservation of mass condition by defining the *mass of a sink* at time t to be the total mass of particles annihilated in the sink between time zero and time t. When sinks coalesce, their masses add up. It will be convenient to assume that sinks do not disappear in the situations when they stop accumulating mass (i.e., when the initial velocity field is discontinuous, as in Sect. 6). In these situations, we assume informally that the sinks are being pushed by the system particles. Formally, there exists three cases depending on the occupancy of a neighborhood of $\sigma(t)$. If there exists an empty neighborhood around the sink coordinate $\sigma(t)$, the sink is considered

at rest – its coordinate does not change. If only the left neighborhood of $\sigma(t)$ is empty, and the right adjacent velocity is negative:

$$v(\sigma_+, t) := \lim_{x \downarrow \sigma(t)} v(x,t) < 0,$$

the sink at $\sigma(t)$ moves with velocity $v(\sigma_+, t)$. A similar rule is applied to the case of right empty neighborhood. A formal description of the sink speed is given below in Eq. (19). Accordingly, it is convenient to think of the dynamics of *massive particles*, each of which corresponds to a sink that can annihilate particles and hence accumulate mass, or be pushed by the system particles without annihilation and mass accumulation.

We refer to a trajectory of a massive particle as a *shock wave*. The appearance, motion, and subsequent coalescence of massive particles can be described by a time oriented *shock wave forest*. In particular, the coalescence of massive particles under initial conditions with a finite number of sink sources is described by a finite forest.

5.2. **Basic constraints on ballistic annihilation dynamics.** Suppose $x_- < x_+$ are such that $v(x_-) > v(x_+)$. Assume that density $g(x)$ is positive, and suppose there is only one sink source $x^* \in (x_-, x_+)$. In order for x_- and x_+ to annihilate each other in the sink originated at x^* at time $t > t^*$ we need the following:

(i) Collision at time t:

$$x_- + tv(x_-) = x_+ + tv(x_+).$$

(ii) The mass between x_- and x^* annihilates the mass between x^* and x_+:

$$\int_{x_-}^{x^*} g(x)\,dx = \int_{x^*}^{x_+} g(x)\,dx.$$

(iii) Neither x_- nor x_+ is annihilated before time t.

From conditions (i) and (ii), we obtain the velocity of the sink at time t:

$$\frac{d}{dt}\sigma(t) = \frac{v(x_-)\frac{g(x_-)}{1+tv'(x_-)} + v(x_+)\frac{g(x_+)}{1+tv'(x_+)}}{\frac{g(x_-)}{1+tv'(x_-)} + \frac{g(x_+)}{1+tv'(x_+)}}. \tag{19}$$

Indeed, let $x_- = x_-(t)$ and $x_+ = x_+(t)$ be the left and the right points annihilating each other at the location $\sigma(t)$ of the sink at time $t > 0$.

Then, differentiating the equation in condition (i), we obtain

$$\frac{d}{dt}\sigma(t) = x'_-(t) + v\Big(x_-(t)\Big) + tx'_-(t)v'\Big(x_-(t)\Big) \tag{20}$$

$$= x'_+(t) + v\Big(x_+(t)\Big) + tx'_+(t)v'\Big(x_+(t)\Big), \tag{21}$$

while differentiating the balance of mass equation in condition (ii), we get

$$x'_-(t)g\Big(x_-(t)\Big) + x'_+(t)g\Big(x_+(t)\Big) = 0. \tag{22}$$

The above equations (20), (21), and (22) yield (19).

This sink dynamics description is not restricted to $v(x) \in \mathcal{C}^1(\mathbb{R})$, and can be extended to the case of piecewise smooth $v(x)$.

Example 5 (Two velocities, single sink). Suppose $g(x) > 0$ for all $x \in \mathbb{R}$. Let $v(x) = \begin{cases} v_- & \text{if } x \le x^* \\ v_+ & \text{if } x > x^* \end{cases}$, where the constants $v_- > v_+$ and x^* are given. Naturally, x^* is the only sink source and the only sink appears at the sink source at time $t = 0$. Moreover, analogously to (19), one can derive the dynamics of the sink at time t:

$$\frac{d}{dt}\sigma(t) = \frac{v_-g(x_-) + v_+g(x_+)}{g(x_-) + g(x_+)}, \tag{23}$$

where $x_- < x^*$ is the only root of

$$G_t(y) = \int_{x^*}^{y+t(v_- - v_+)} g(x)\,dx - \int_{y}^{x^*} g(x)\,dx,$$

and $x_+ = x_- + t(v_- - v_+)$. Note that $G_t(x)$ is continuous and strictly increasing, and that $G_t(x^*) > 0 > G_t\Big(x^* - t(v_- - v_+)\Big)$.

The dynamics of ballistic annihilation, either in discrete or continuum versions, can be quite intricate and is lacking a general description. The discrete 1-D ballistic annihilation model with two possible velocities $\pm v$ was considered in [18, 9, 8, 19, 13]; the three velocity case (-1, 0, and $+1$) appeared in [17, 44]. The existing analyses focus on the evolution of selected statistics under particular initial conditions. In the following section, we give a complete description of the continuum annihilation dynamics in case of two-valued initial velocity and constant particle density.

6. Continuum 1-D ballistic annihilation: Piece-wise linear potential with unit slopes

Here we study a continuum version of the 1-D ballistic annihilation with two possible initial velocities and constant initial density, i.e. $v(x) = \pm v$ and $g(x,0) \equiv g(x) \equiv g_0$ for $x \in [a,b]$. Since we can scale both space and time, without loss of generality we let $v(x) = \pm 1$ and $g(x) \equiv 1$.

Formally, we consider the space $\mathcal{E}^{\text{ex}}$ of positive piece-wise linear continuous excursions with alternating slopes ± 1 and finite number of segments. We write $\mathcal{E}^{\text{ex}}([a,b])$ for the restriction of this space on the real interval $[a,b]$. We consider an initial potential $\psi(x,0) = \Psi_0(x)$ such that $-\psi(x,0) \in \mathcal{E}^{\text{ex}}([a,b])$; see Fig. 2. This space bears a lot of symmetries that facilitate our analysis.

The dynamics of a system with a simple unit slope potential is illustrated in Fig. 10. Prior to collision, the particles move at unit speed either to the left or to the right, so their trajectories in the (x,t) space are given by lines with slope ± 1 (Fig. 10, top panel, gray lines). The local minima of the potential $\Psi_0(x)$ correspond to the points whose right neighborhood moves to the left and left neighborhood moves to the right with unit speed, hence immediately creating a sink. Accordingly, the sinks appear at $t = 0$ at the local minima of the potential; and those are the only sinks of the system. The sinks move and merge to create a shock wave tree, shown in blue in Fig. 10.

The two white (unshaded) rectangles in the top panel of Fig. 10 correspond to the regions of zero particle density. The segments of the shock wave (blue) that bound these rectangles correspond to the sinks that are being pushed by the system particles, with no annihilation and mass accumulation. The parts of the shock wave that fall within the shaded region correspond to the sinks that annihilate particles and accumulate mass.

Observe that the domain $[a,b]$ is partitioned into non-overlapping subintervals with boundaries x_j such that the initial particle velocity assumes alternating values of ± 1 within each interval, with boundary values $v(a,0) = v(a) = 1$ and $v(b,0) = v(b) = -1$. Because of the choice of potential $\Psi_0(x)$, we have

$$\int_a^b v(x)\,dx = \Psi_0(b) - \Psi_0(a) = 0,$$

i.e. the total length of the subintervals with the initial velocity -1 equals the total length of the subintervals with the initial velocity 1. For a finite interval $[a,b]$, there exists a finite time $t_{\max} = (b-a)/2$ at which

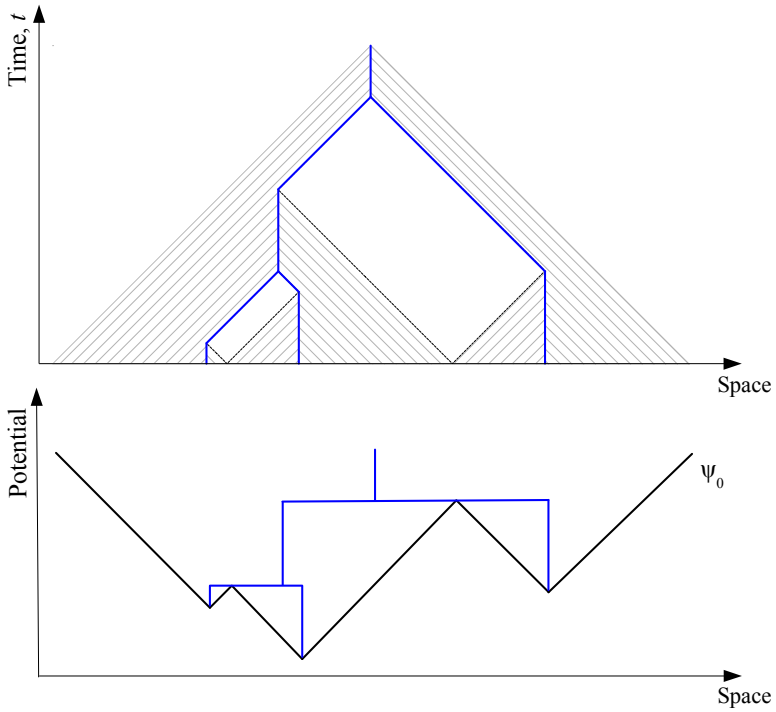

FIGURE 10. Shock wave tree in a model with a unit slope potential: an illustration. (Top panel): Space-time dynamics of the system. Trajectories of particles are illustrated by gray lines. The trajectory of massive particles (coalescing sinks) is shown by blue line – this is the graphical representation $\mathcal{G}^{(x,t)}(\Psi_0)$ of the shock wave tree $S(\Psi_0)$. Notice the appearance of empty regions (zero particle density) in the space-time domain. (Bottom panel): Initial unit slope potential $\Psi_0(x)$ with three local minima (black line) and a graphical representation $\mathcal{G}^{(x,\psi)}(\Psi_0)$ of the shock wave tree (blue line) in the phase space $(x, \psi(x,t))$.

all particles aggregate into a single sink of mass $m = (b-a) = 2\,t_{\max}$; see discussion below. We assume that the density of particles vanishes outside of $[a,b]$ and only consider the solution on the time interval $[0, t_{\max}]$.

6.1. **Shock waves.** For our fixed choice of the initial particle density $g(x) \equiv 1$, the model dynamics is completely determined by the potential $\Psi_0(x)$. We will be particularly interested in the dynamics of shock waves. The trajectories of massive particles can be described by a set

(Fig. 10, top panel)

$$\mathcal{G}^{(x,t)}(\Psi_0) = \Big\{\Big(x,t\Big) \in \mathbb{R}^2 \,:\, \exists \text{ a massive particle at } (x,t)\Big\}$$

in the system space-time domain $(x,t) : x \in [a,b],\ t \in \Big[0,(b-a)/2\Big]$. For any two points $(x_i,t_i) \in \mathcal{G}^{(x,t)}(\Psi_0)$, $i=1,2$, connected by a self-avoiding path γ within $\mathcal{G}^{(x,t)}(\Psi_0)$, we define the distance between them as

$$d^{(x,t)}\Big((x_1,t_1),(x_2,t_2)\Big) = \int\limits_{\gamma} |dt| = 2t^* - t_1 - t_2, \tag{24}$$

where

$$t^* := \max\{t : (x,t) \in \gamma\}.$$

Equivalently, the distance between two points within an uninterrupted run of a massive particle (i.e., without merging with another particle) is defined as their nonnegative time increment; this induces the distance $d^{(x,t)}$ on $\mathcal{G}^{(x,t)}(\Psi_0)$.

Similarly, the trajectories of the massive particles can be described by a set (Fig. 10, bottom panel)

$$\mathcal{G}^{(x,\psi)}(\Psi_0) = \Big\{\Big(x,\psi(x,t)\Big) \in \mathbb{R}^2 \,:\, \exists \text{ a massive particle at } (x,t)\Big\}$$

in the system phase space $(x,\psi(x,t)) :\ x \in [a,b],\ t \in \Big[0,(b-a)/2\Big]$. For any two points $(x_i,\psi_i) \in \mathcal{G}^{(x,\psi)}(\Psi_0)$, $i=1,2$, connected by a self-avoiding path γ within $\mathcal{G}^{(x,\psi)}(\Psi_0)$, we define the distance between them as

$$d^{(x,\psi)}\Big((x_1,\psi_1),(x_2,\psi_2)\Big) = \int\limits_{\gamma} \Big(|dt| + |dx|\Big). \tag{25}$$

Equivalently, one can consider the L^1 distance between the points along path γ; this induces the distance $d^{(x,\psi)}$ on $\mathcal{G}^{(x,\psi)}(\Psi_0)$.

6.2. **Tree structure of shock waves.** Here we show that the shock waves $\mathcal{G}^{(x,\psi)}$ and $\mathcal{G}^{(x,t)}$ in our model have a finite binary tree structure. Multiple useful symmetries of these trees are summarized in Lem. 5. The general construction is presented in Sect. 6.2.3; it is based on a W-shaped potential discussed in Sect. 6.2.2. To develop intuition and cover all possible cases, we begin with a simple V-shaped potential.

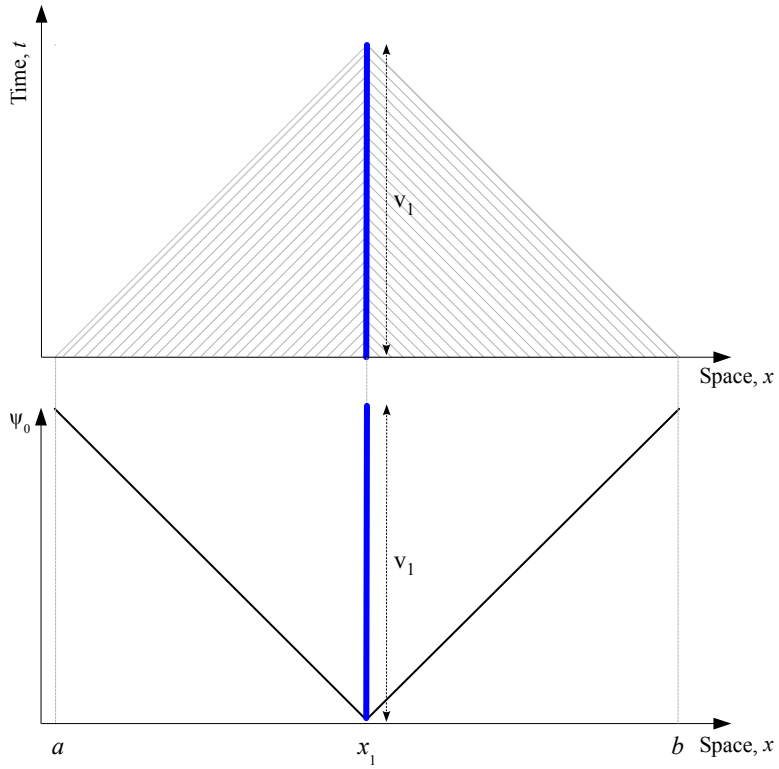

FIGURE 11. A V-shaped potential on interval $[a, b]$. (Bottom): The potential Ψ_0 (black line) and the shock wave in the phase space (x, ψ) (blue segment). (Top): The space-time portrait. The system occupies a triangular (shaded) region in the (x, t) space. Thin hatching illustrates the trajectories of regular particles. Blue vertical segment show the trajectory of the massive particle. The length of this segment in both panels is $\mathrm{v}_1 = (b - a)/2$.

6.2.1. *V-shaped potential.* Let $x_1 = c = (a + b)/2$ be the center of the segment $[a, b]$. Consider the simplest V-shaped potential that consists of a negative segment on $[a, c]$ and a positive segment on $[c, b]$; see Fig. 11. In this case, there exists a single massive particle that originates at $t = 0$ at the point $(c, \Psi_0(c))$. In x-space, it remains at rest and accumulates mass at rate 2 during the time interval of duration $(b - a)/2$, which reflects accumulation of regular particles that merge into the massive particle from left and right. After this, the mass of the particle is $(b - a)$, which reflects complete accumulation of all regular particles from the interval $[a, b]$.

In the phase space (Fig. 11, bottom panel), the trajectory of the massive particle corresponds to a vertical segment of length $\mathrm{v}_1 = (b - a)/2$ between points $(x_1, \Psi_0(x_1))$ and $(x_1, \Psi_0(x_1) + \mathrm{v}_1)$. The trajectory of each regular particle is a horizontal line from the particle's initial position $(x, \psi(x, 0))$ to the point of merging with the massive particle at $(x_1, \psi(x, 0))$.

In the space-time domain (Fig. 11, top panel) the trajectory of the massive particle is a vertical segment between points $(x_1, 0)$ and (x_1, v_1). The trajectories of regular particles, each of which moves with its initial velocity until merging with the massive particle, are shown by thin diagonal lines.

To summarize, in the case of a V-shaped potential, each of the shock waves $\mathcal{G}^{(x,\psi)}$ and $\mathcal{G}^{(x,t)}$ is a vertical interval of length v_1 (blue lines in Fig. 11). The distances $d^{(x,\psi)}$ of (25) and $d^{(x,t)}$ of (24) coincide with the Lebesgue measure on these intervals.

6.2.2. *W-shaped potential.* Consider now a negative excursion on $[a, b]$ with exactly two local minima at x_1, x_3 and the only local maxima at x_2, with $a < x_1 < x_2 < x_3 < b$, see Fig. 12. There exist two massive particles that originate at $t = 0$ at points x_1 and x_3. The massive particle at x_1 remains at rest and accumulates mass at rate 2 during time interval of duration $\mathrm{v}_1 = \Psi_0(x_2) - \Psi_0(x_1)$. At instant $t = \mathrm{v}_1$ the right neighborhood of the massive particle at x_1 becomes empty, and it starts moving at unit speed to the right. Similarly, the massive particle at x_3 remains at rest and accumulates mass at rate 2 during time interval of duration $\mathrm{v}_3 = \Psi_0(x_2) - \Psi_0(x_3)$. At instant $t = \mathrm{v}_3$ the left neighborhood of the massive particle at x_3 becomes empty, and it starts moving at unit speed to the left. The two massive particles move toward each other until they merge to form a new massive particle of mass $2(\mathrm{v}_1 + \mathrm{v}_3)$. We denote by h_i, $i = 1, 3$ the durations of these respective movements. Since both right and left neighborhoods of the new massive particle are occupied by regular particles, the particle remains at rest for some time.

The following lemma summarizes this discussion and describes the shock trajectories $\mathcal{G}^{(x,\psi)}(\Psi_0)$ and $\mathcal{G}^{(x,t)}(\Psi_0)$. This is the basic element for constructing a general potential solution in Sect. 6.2.3.

Lemma 3 (**Shock tree of a W-shaped potential**). *For a W-shaped potential described above (and illustrated in Fig. 12) we have:*

(a) *The shock trajectory $\mathcal{G}^{(x,\psi)}(\Psi_0)$ in the phase space has the bracket tree shape that consists of two leaves and a root edge (Fig. 12, bottom panel). Each leaf corresponds to the dynamics of one of*

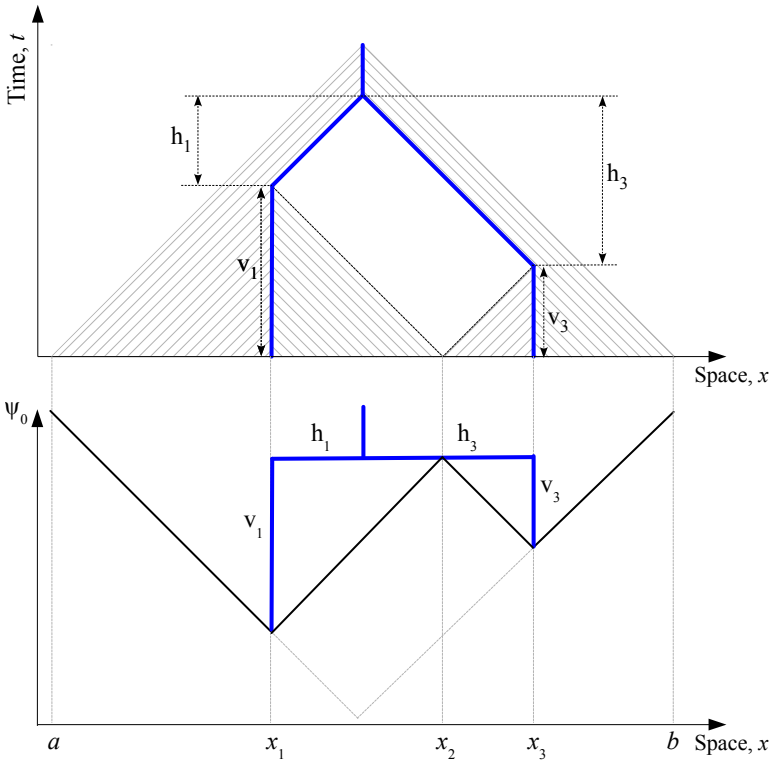

FIGURE 12. A W-shaped potential. (Bottom): The potential Ψ_0 (solid black) and the shock in the phase space (x, ψ) (blue). (Top): The space-time portrait. The system occupies a shaded region in the (x, t) space, bounded by a triangle that corresponds to the V-shaped potential on the interval $[a, b]$, as in Fig. 11. Notice the appearance of an empty rectangular region in the space-time portrait that corresponds to (x, t) locations with no particles. Thin hatching illustrates the trajectories of regular particles. Blue lines show the trajectories of massive particles.

the two initial massive particles; the root edge corresponds to the dynamics of the final massive particle. Each leaf consists of a vertical segment between points $(x_i, \Psi_0(x_i))$ *and* $(x_i, \Psi_0(x_2))$*, and a horizontal segment between points* $(x_i, \Psi_0(x_2))$ *and* $(c, \Psi_0(x_2))$*, for* $i = 1, 3$*. The stem consists of a vertical segment between points* $(c, \Psi_0(x_2))$ *and* $(c, \Psi_0(a))$*. Here* $c = (a + b)/2$ *is the center of the interval* $[a, b]$*.*

(b) *In the space-time domain* (x, t)*, the system occupies a cone* $\mathcal{C}$ *that has the shape of a right triangle with the hypotenuse on the*

interval $\{x,t\} = \{[a,b],0\}$ *and the legs merging at the point* (c,c). *The shock trajectory* $\mathcal{G}^{(x,t)}(\Psi_0)$ *forms an inverted Y-shaped tree shown in Fig. 12 (top panel) that consists of two leaves and a stem. Each leaf corresponds to the dynamics of one of the two initial massive particles; the stem corresponds to the dynamics of the final massive particle. Each leaf consists of a vertical segment between points* $(x_i,0)$ *and* (x_i,v_i), *and a slanted segment between points* (x_i,v_i) *and* $(c,\mathrm{v}_1+\mathrm{v}_3)$, *for* $i=1,3$. *The stem consists of a vertical segment between points* $(c,\mathrm{v}_1+\mathrm{v}_3)$ *and* (c,c). *There exists a rectangular empty region (no particles) with vertices at the points (clock-wise from the bottom point):* $(x_2,0)$, (x_1,v_1), $(c,\mathrm{v}_1+\mathrm{v}_3)$, *and* (x_3,v_3).

(c) *The regular particles move in the direction of their initial velocities until they merge with a massive particle. A regular particle* x *in the interval* $[x_1-\mathrm{v}_1, x_1+\mathrm{v}_1=x_2)$ *merges with the massive particle at point* x_1 *at time instant* $t=|x_1-x|$. *A regular particle* x *in the interval* $(x_3-\mathrm{v}_3=x_2, x_3+\mathrm{v}_3]$ *merges with the massive particle at point* x_3 *at time instant* $t=|x_3-x|$. *A regular particle* x *in the intervals* $[a,x_1-\mathrm{v}_1)$ *and* $(x_3+\mathrm{v}_3,b]$ *merges with the massive particle at point* $(a+b)/2$ *at time instant* $t=|(a+b)/2-x|$. *The regular particle at* x_2 *merges the massive particle at* x_1 *(*x_3*) if the potential is left (right) continuous at time instant* $t=x_2-x_1$ *(*$t=x_3-x_2$*).*

(d) *The metric spaces* $\left(\mathcal{G}^{(x,t)}(\Psi_0), d^{(x,t)}\right)$ *and* $\left(\mathcal{G}^{(x,\psi)}(\Psi_0), d^{(x,\psi)}\right)$ *are isometric binary trees.*

Proof. The statements follow from model definition and elementary geometric properties of a W-shaped potential illustrated in Fig. 12. □ □

Next, we make a symmetry observation, which helps to extend our geometric construction of the shock tree to an arbitrary potential. We define the *basin* $\mathcal{B}_2$ for the local maximum at x_2 as the shortest interval that contains x_2 and supports a non-positive excursion in $\Psi_0(x)$. Formally, $\mathcal{B}_2=[x_2^{\mathrm{left}}, x_2^{\mathrm{right}}]$, where

$$x_2^{\mathrm{right}} = \inf\{x : x>x_2 \text{ and } \Psi_0(x)>\Psi(x_2)\},$$

$$x_2^{\mathrm{left}} = \sup\{x : x<x_2 \text{ and } \Psi_0(x)>\Psi(x_2)\}.$$

The basin length is denoted by $|\mathcal{B}_2| = x_2^{\mathrm{right}} - x_2^{\mathrm{left}}$.

Lemma 4 (**Symmetry lemma**). *Let* $\mathrm{v}_i, \mathrm{h}_i$ *for* $i=1,3$ *be the lengths of the vertical and horizontal segments, respectively, of the leaves of the*

shock tree for a W-shaped potential:

$$\mathrm{v}_i = \Psi_0(x_2) - \Psi_0(x_i), \quad \mathrm{h}_i = |(a+b)/2 - x_i|.$$

Then

$$\mathrm{h}_1 = \mathrm{v}_3, \quad \mathrm{h}_3 = \mathrm{v}_1$$

and

$$\mathrm{v}_i + \mathrm{h}_i = |\mathcal{B}_2|/2 = (b-a)/2 - (\Psi_0(a) - \Psi_0(x_2)).$$

Proof. By elementary geometric properties of the shock wave tree for a W-shaped potential illustrated in Fig. 12. □ □

Lemma 4 implies that after instant $t = |\mathcal{B}_2|/2$ when the massive particles that originate at x_1 and x_3 merge, the process dynamics is indistinguishable from that of the V-shaped potential on $[a, b]$. This loss of memory property is used below to construct the shock tree in a general case, using a recursive construction by the number of local maxima of the potential.

6.2.3. *General potential.* This section considers a potential $\Psi_0(x) \equiv \Psi_1(x)$ with $-\Psi_1(x) \in \mathcal{E}^{\mathrm{ex}}([a, b])$ and such that $\Psi_0(x)$ has distinct values of the local maxima.

We begin by extending the *basin* definition of Sect. 6.2.2. Specifically, for each local extremum x_j of $\Psi_0(x)$, we define its *basin* $\mathcal{B}_j$ as the shortest interval that contains x_j and supports a non-positive excursion of $\Psi_0(x)$. Formally, $\mathcal{B}_j = [x_j^{\mathrm{left}}, x_j^{\mathrm{right}}]$, where

$$x_j^{\mathrm{right}} = \inf\Big\{x : x > x_j \text{ and } \Psi_0(x) > \Psi(x_j)\Big\},$$

$$x_j^{\mathrm{left}} = \sup\Big\{x : x < x_j \text{ and } \Psi_0(x) > \Psi(x_j)\Big\}.$$

The basin's length is $\Big|\mathcal{B}_j\Big| = x_j^{\mathrm{right}} - x_j^{\mathrm{left}}$. Point $c_j = (x_j^{\mathrm{right}} + x_j^{\mathrm{left}})/2$ denotes the center of the basin $\mathcal{B}_j$. Additionally, we let

$$\mathrm{v}_j = \Psi_0(x_{\mathsf{parent}(j)}) - \Psi_0(x_j) \quad \text{and} \quad \mathrm{h}_j = \Big|\mathcal{B}_{\mathsf{sibling}(j)}\Big|/2.$$

We observe that the basin $\mathcal{B}_j$ for a local minimum x_j coincides with its coordinate: $\mathcal{B}_j = \{x_j = x_j^{\mathrm{left}} = x_j^{\mathrm{right}}\}$.

The shock tree for the V-shaped potential was constructed in Sect. 6.2.1. If the potential is not V-shaped, it has $n \geq 1$ local maxima. We assume that the values of the local maxima are distinct. Consider the basins that correspond to the local maxima of $\Psi_1(x)$ and re-index them according to their lengths, from shortest to longest:

$$|\mathcal{B}_1| < |\mathcal{B}_2| < \cdots < |\mathcal{B}_n|.$$

Let $t_i = |\mathcal{B}_i|/2$. For each basin $\mathcal{B}_i$ we define the corresponding *space-time cone* $\mathcal{C}_i$ that has the shape of a right triangle with hypotenuse $\{x, t\} = \{\mathcal{B}_i, 0\}$ and legs merging at the point $(x_i^{\text{left}} + t_i, t_i)$; see Fig. 14.

It is readily seen that the shortest basin $\mathcal{B}_1$ necessarily supports a W-shaped potential. We construct the shock tree for the regular particles within the space interval $\mathcal{B}_1$ during the time interval $[0, t_1]$, using the W-shaped potential construction of Lemma 3. Hence, we describe the system dynamics in the space-time cone $\mathcal{C}_1$.

Consider now the *unfolded* potential $\Psi_2(x)$ that coincides with $\Psi_1(x)$ outside of $\mathcal{B}_1$ and has a V-shaped form on $\mathcal{B}_1$; Fig. 13. (This potential is obtained by "unfolding" the inner local maximum of the W-shaped potential within the basin $\mathcal{B}_1$, hence its name.) By construction, and using Lemma 3, the trees that correspond to the potentials Ψ_1 and Ψ_2 coincide outside of the cone $\mathcal{C}_1$ in the space-time domain. The potential $\Psi_2(x)$ has $n - 1$ local maxima. Its shortest basin is $\mathcal{B}_2$; it necessarily corresponds to a W-shaped potential within $\Psi_2(x)$. We use $\Psi_2(x)$ to construct the space-time tree on $\mathcal{C}_2$, using the W-shaped potential algorithm of Lemma 3. The resulting tree is only considered within the space-time subregion $\mathcal{C}_2 \setminus \mathcal{C}_1$. The union of this tree and the tree constructed in the initial step within $\mathcal{C}_1$ results in the tree within $\mathcal{C}_1 \cup \mathcal{C}_2$.

Consider now a set of unfolded potentials $\Psi_i(x)$, $i = 3, \ldots, n$, such that $\Psi_i(x)$ coincides with $\Psi_{i-1}(x)$ on $[a, b] \setminus \mathcal{B}_i$ and forms a V-shaped negative excursion on $\mathcal{B}_{i-1}$, see Fig. 13. By construction, the shortest basin within every $\Psi_i(x)$ is $\mathcal{B}_i$, and it supports a W-shaped potential. We apply the W-shaped potential algorithm to each potential $\Psi_i(x)$ within the basin $\mathcal{B}_i$, hence consecutively extending the shock tree construction to the space-time subsets

$$\bigcup_{j=1}^{i} \mathcal{C}_j.$$

At instant t_n there exists a single massive particle within a V-shaped potential $\Psi_n(x)$ on $[a, b]$, which is treated according to the V-shaped potential construction. This completes the space-time tree construction.

Figure 14 illustrates the above process for a potential with 4 local maxima. The space-time cones $\mathcal{C}_i$, $i = 1, \ldots, 5$ are labeled in the figure. Here, the largest cone $\mathcal{C}_5$ corresponds to the entire space-time system's domain.

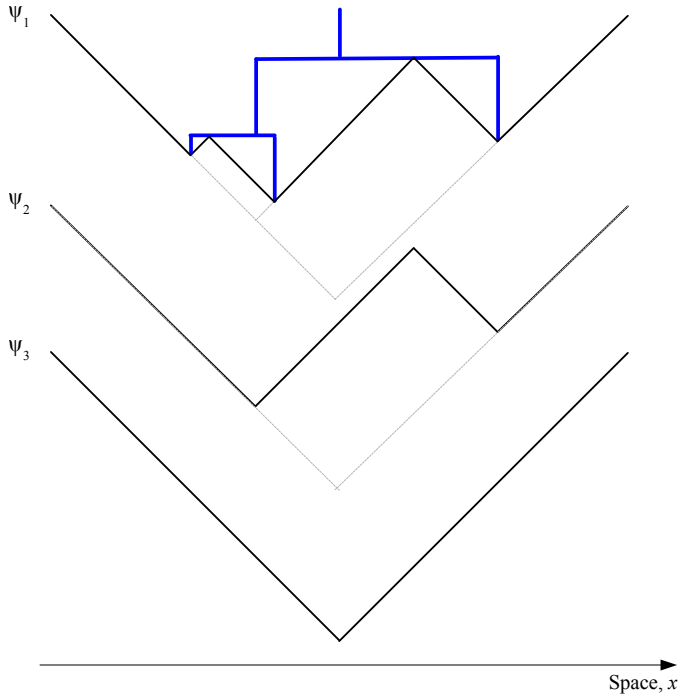

FIGURE 13. Potential unfolding: an illustration. The potential $\Psi_2(x)$ is an unfolding of $\Psi_1(x)$, and $\Psi_3(x)$ is an unfolding of $\Psi_2(x)$. The shock tree in the phase space is shown (blue segments) next to the initial potential $\Psi_1(x)$. The potentials $\Psi_{2,3}(x)$ are arbitrarily shifted in vertical direction for visual convenience.

Observe that the graphical shock trees $\mathcal{G}^{(x,\psi)}$ and $\mathcal{G}^{(x,t)}$ in the phase space and in the space-time domain have the same combinatorial structure and planar embedding, coinciding with that of $S(\Psi_0)$ (recall that embedding only involves ordering between the offspring of the same parent, and is different from a particular graphical representation of a tree). The graphical trees become metric spaces, when equipped with the distances $d^{(x,\psi)}$ of (25) and $d^{(x,t)}$ of (24), respectively.

The following statement summarizes the correspondence between the dynamics of the sinks and the graphical tree $\mathcal{G}^{(x,\psi)}(\Psi_0)$.

Lemma 5 (Shock tree). *Consider function $\Psi_0(x)$ such that $-\Psi_0(x) \in \mathcal{E}^{\text{ex}}$ and $\Psi_0(x)$ has distinct values of local maxima. Let $\mathcal{G} \equiv \mathcal{G}^{(x,\psi)}(\Psi_0)$ be the graphical shock wave of a continuum annihilation dynamics with unit density $g(x) \equiv 1$ and initial potential $\Psi_0(x)$. Then metric space $\left(\mathcal{G}^{(x,\psi)}(\Psi_0), d^{(x,\psi)}\right)$ is isometric to a finite binary tree with edge lengths from $\mathcal{BL}^{|}_{\text{plane}}$. In addition, the following statements hold:*

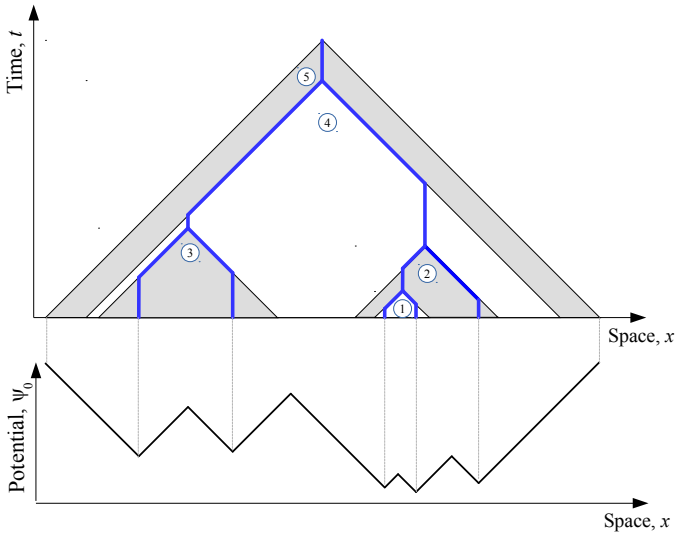

FIGURE 14. Iterative solution construction: an illustration for a potential $\Psi_0(x)$ (bottom panel) with four local maxima. (Top): Space-time cones $\mathcal{C}_1, \ldots, \mathcal{C}_4$ that correspond to the basins $\mathcal{B}_1, \ldots, \mathcal{B}_4$. Blue segments show the shock tree. The cone $\mathcal{C}_5$ corresponds to the V-shaped potential on the whole space interval.

a) *There exists a one-to-one correspondence between points $z \in \mathcal{G}$ and space-time locations (x_z, t_z) of sinks. In particular, there exists a one-to-one correspondence between the sinks at instant $t = 0$ and the leaves of $\mathcal{G}$, and a one-to-one correspondence between the instants when two sink merge and the internal vertices of $\mathcal{G}$.*
b) *Every sink at any time can either be at rest and accumulate mass at rate 2, or move with a unit speed with no mass accumulation. A point on any vertical segment of $\mathcal{G}$ corresponds to a sink at rest. A point on any horizontal segment of $\mathcal{G}$ corresponds to a sink in motion.*
c) *Suppose a point $z \in \mathcal{G}$ corresponds to a sink with mass m_z at location (x_z, t_z). Then t_z equals the length $d^{(x,\psi)}$ from z to any descendant leaf within $\mathcal{G}$. The mass $m_z \le 2t_z$ equals double the total length of the vertical segments of the subtree $\Delta_{z,\mathcal{G}} \subset \mathcal{G}$ descendant to z. Furthermore, $m_z = 2\,t_z$ if and only if z is located on a vertical segment of $\mathcal{G}$.*
d) *The length h_j of a horizontal segment equals the total length of the vertical segments within its sibling subtree. (Here, the two complete descendant subtrees of $\mathcal{G}$ rooted at the same internal*

vertex are called sibling subtrees.) In other words, the time spent by a sink in uninterrupted motion prior to a collision with another sink equals half the mass of the sink with which it collides.

Proof. Items (a), (b) follow from the constructions of in Sects. 6.2.1, 6.2.2, 6.2.3. Items(c), (d) follow from recursive application of Lem. 4 to unfolding potentials used in the construction. □ □

Example 6. As an example of Lemma 5(d), consider the model of Fig. 15 that has two pairs of sibling trees. The first pair is formed by the complete descendant subtrees of vertex 2. Here, $\mathrm{h}_1 = \mathrm{v}_3$ and $\mathrm{h}_3 = \mathrm{v}_1$. The second pair is formed by the complete descendant subtrees of vertex 4. Here, $\mathrm{h}_2 = \mathrm{v}_5$ and $\mathrm{h}_5 = \mathrm{v}_1 + \mathrm{v}_2 + \mathrm{v}_3$.

Remark 1. A statement analogous to that of Lem. 5 holds for the graphical shock wave $\mathcal{G} = \mathcal{G}^{(x,t)}(\Psi_0)$ and the respective metric space $\Big(\mathcal{G}^{(x,t)}(\Psi_0), d^{(x,t)}\Big)$ in the space-time domain. Specifically, item (a) holds verbatim. In item (b) one needs to replace "horizontal segment" with "slanted segment". In item (c) one needs to replace $d^{(x,\psi)}$ with $d^{(x,t)}$. In item (d) one needs to replace "The length h_j of a horizontal segment..." with "The height h_j of a slanted segment...".

Lemma 6 (**Shock wave tree**)**.** *Suppose that $-\Psi_0 \in \mathcal{E}^{\mathrm{ex}}$ and the local maxima of Ψ_0 have distinct values. Then the metric spaces $\Big(\mathcal{G}^{(x,t)}(\Psi_0), d^{(x,t)}\Big)$ and $\Big(\mathcal{G}^{(x,\psi)}(\Psi_0), d^{(x,\psi)}\Big)$ are finite binary trees. Furthermore, they are isomeric to a unique binary tree from $\mathcal{BL}^{|}_{\mathrm{plane}}$ that we denote by $S(\Psi_0)$.*

Proof. The statement follows from Lem. 5 and Rem 1. In particular, the uniqueness is established by noticing that a tree from $\mathcal{BL}^{|}_{\mathrm{plane}}$ is uniquely specified by the parent-offspring relations among vertices and the edge lengths $\mathrm{v}_i + \mathrm{h}_i$. □ □

We refer to the trees of Lem. 6 as *graphical trees* $\mathcal{G}^{(x,t)}(\Psi_0)$ and $\mathcal{G}^{(x,\psi)}(\Psi_0)$; they are two alternative graphical representations of the tree $S(\Psi_0)$ that we refer to as the *shock wave tree*.

6.3. **Embedding of shock wave tree in the model potential.** With our particular choice of the initial potential (a negative excursion with unit slopes), the combinatorial structure and the planar embedding of the shock wave tree coincide with that of the level set tree $T = \textsc{level}\Big(-\Psi_0\Big)$ of the initial potential, as we state in the following theorem.

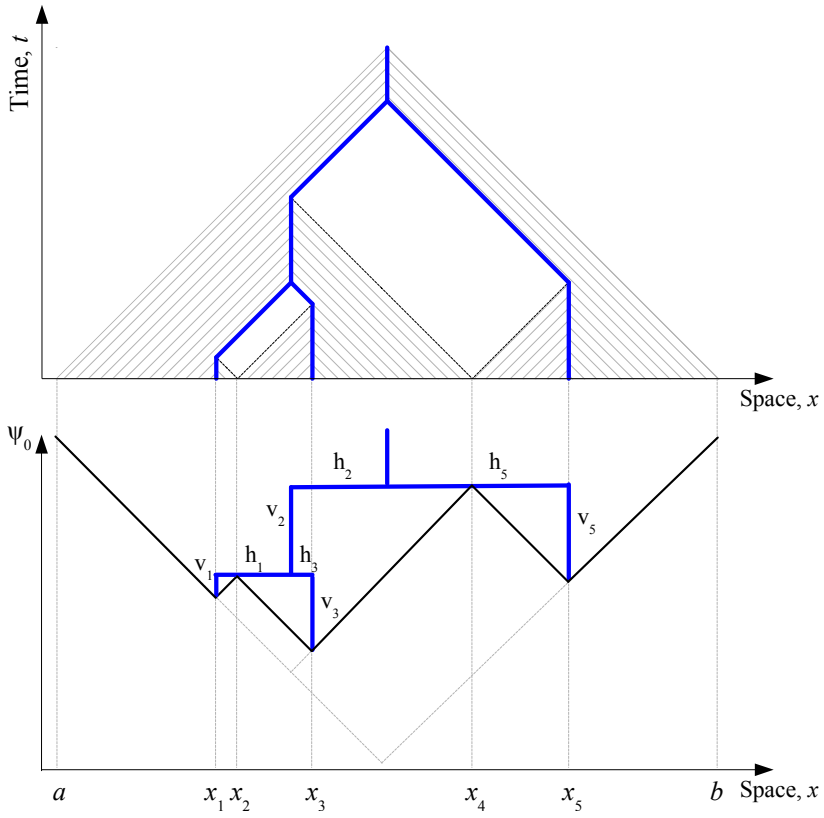

FIGURE 15. Shock tree for a piece-wise linear potential with two local maxima. (Top): The shock tree in space-time domain (blue). Hatching illustrates motion of regular particles. There exist two empty rectangular areas, each corresponding to one of the local maxima. The panel illustrates indexing of the tree vertices. (Bottom): Potential $\Psi_0(x)$ (black) and the shock tree in the phase space (blue). The panel illustrates the labeling of vertical (v_j) and horizontal (h_j) segments of the tree.

Theorem 4 (**Shock wave is a level set tree**). *Suppose* $g(x) \equiv 1$ *and the initial potential* $\Psi_0(x)$ *is such that* $-\Psi_0(x) \in \mathcal{E}^{\mathrm{ex}}$ *and* $\Psi_0(x)$ *has distinct values of local maxima. Then*

$$\textsc{p-shape}\Big(\textsc{level}\,(-\Psi_0)\Big) = \textsc{p-shape}\Big(S(\Psi_0)\Big).$$

Proof. Considering the level set tree of a negative potential reflects the fact that the level set tree is constructed top to bottom (leaves correspond to local maxima), and the shock wave tree is constructed bottom to top (leave correspond to local minima).

Observe that the statement is true for a V-shaped potential (see Sect. 6.2.1, Fig. 11), whose level set tree is comprised by a single edge, and a W-shaped potential (see Sect. 6.2.2, Fig. 12), whose level set tree is a Y-shaped planted binary tree with two leaves.

The general statement follows from the recursive shock wave tree construction presented in Sect. 6.2.3 and the definition of the level set tree in Sect. 2.2. Specifically, we start with a Y-shaped tree that corresponds to a W-shaped potential within the cone $\mathcal{C}_1$ (see Sect. 6.2.3, Fig. 14 for definition of the cone). The k-th unfolding of the initial potential $\Psi_0(x)$ produces a shock wave within the cone $\mathcal{C}_{k+1}$. This is a planted binary tree with $k+2$ leaves. This tree is obtained by replacing one of the leaves of the Y-shaped tree that corresponds to an unfolded W-shaped potential within the cone $\mathcal{C}_{k+1}$ with the tree with $k+1$ leaves constructed within the cone $\mathcal{C}_k$. The statement of the theorem now follows from examining the level set trees for each W-shaped potential and combining them according to the unfolding process of Sect. 6.2.3. □ □

Theorem 4 implies that there is one-to-one correspondence between internal local maxima of $\Psi_0(x)$ and internal non-root vertices of $S(\Psi_0)$. There is also a one-to-one correspondence between local minima and the leaves. We label the tree vertices with the indices j that correspond to the enumeration of the local extrema x_j of $\Psi_0(x)$; see Fig. 15. We write $\mathsf{parent}(i)$ for the index of the parent vertex to vertex i; $\mathsf{right}(i)$ and $\mathsf{left}(i)$ for the indices of the right and the left offsprings of an internal vertex i; and $\mathsf{sibling}(i)$ for the index of the unique vertex that has the same parent as vertex i.

We are now ready to describe the metric structure of the shock tree $S(\Psi_0)$ and a constructive embedding $\mathcal{G}^{(x,\psi)}(\Psi_0)$ of the tree $S(\Psi_0)$ into the system's phase space (and hence into the potential function).

Metric tree structure. The length l_j of the parental edge of a non-root vertex j within $S(\Psi_0)$ is given by $l_j = \mathrm{v}_j + \mathrm{h}_j$.

Graphical shock tree in the phase space. The tree $\mathcal{G}^{(x,\psi)}(\Psi_0)$ is the union of the following vertical and horizontal segments:

(v) For every local extremum x_j of $\Psi_0(x)$ there exists a vertical segment from $(c_j, \Psi_0(x_j))$ to $(c_j, \Psi_0(x_j) + \mathrm{v}_j)$.

(h) For every local maximum x_j of $\Psi_0(x)$ there exists a horizontal segment of length $\mathrm{h}_{\mathsf{left}(j)} + \mathrm{h}_{\mathsf{right}(j)}$ from $(c_{\mathsf{left}(j)}, \Psi_0(x_j))$ to $(c_{\mathsf{right}(j)}, \Psi_0(x_j))$.

Figure 15 shows the graphical shock trees $\mathcal{G}^{(x,\psi)}$ and $\mathcal{G}^{(x,t)}$ for an initial potential with two local maxima and three local minima, and illustrates the labeling of vertical (v_j) and horizontal (h_j) segments of the tree.

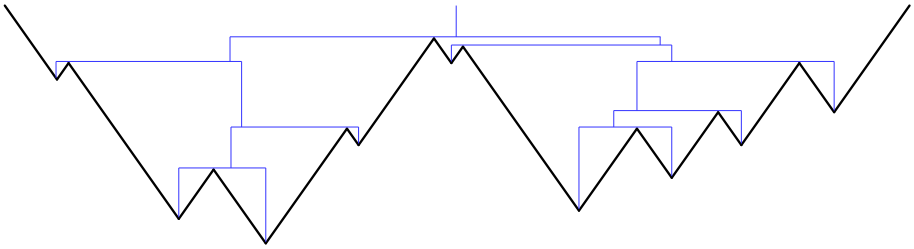

FIGURE 16. Graphical representation $\mathcal{G}^{(x,\psi)}(\Psi_0)$ (blue) of the shock wave tree $S(\Psi_0)$ for initial potential $\Psi_0(x)$ with nine local minima (black). There are nine sinks that correspond to the leaves of the tree. The trajectory of each sink can be traced by going from the corresponding leaf to the root of the tree.

Figure 16 shows an example of the graphical tree $\mathcal{G}^{(x,\psi)}$ for an initial potential with nine local minima (and, hence, with nine initial sinks).

Consider a tree $\mathcal{V}(\Psi_0) \in \mathcal{BL}^{|}_{\text{plane}}$ that has the same planar combinatorial structure as $S(\Psi_0)$, and the length of the parental edge of vertex j is given by $l_j = \mathrm{v}_j$. Informally, this is a tree that consists of the vertical segments of the graphical tree $\mathcal{G}^{(x,\psi)}(\Psi_0)$ (Fig. 10, bottom). We have the following corollary of Thm. 4.

Corollary 3. *Suppose $g(x) \equiv 1$ and potential $\Psi_0(x)$ is such that $-\Psi_0(x) \in \mathcal{E}^{\text{ex}}$ and $\Psi_0(x)$ has distinct values of local maxima. Then*

$$\mathcal{V}(\Psi_0) = \textit{LEVEL}\,(-\Psi_0)\,.$$

Proof. Follows from construction of the shock wave tree in Sect. 6.2.3 and construction of the level set tree in Sect. 2.2. Considering a negative potential reflects the fact that the level set tree is constructed top to bottom (leaves correspond to local maxima), and the shock tree is constructed bottom to top (leave correspond to local minima). □ □

6.4. **Ballistic annihilation as generalized pruning.** This section shows that the dynamics of continuum ballistic annihilation with constant initial density and unit-slope potential is equivalent to the generalized dynamical pruning of either the shock wave tree (Thm. 5) or the level set tree of the potential (Thm. 6).

Suppose a tree $T \in \mathcal{BL}^{|}_{\text{plane}}$ has a particular graphical representation $\mathcal{G}_T \in \mathbb{R}^2$ implemented by a bijective isometry $f : T \to \mathcal{G}_T$ that maps the root of T into the root of $\mathcal{G}_T$. We extend the notion of the generalized dynamical pruning $\mathcal{S}_t(\varphi, \mathcal{G}_T)$ for the graphical tree $\mathcal{G}_T$ by considering

the f-image of $\mathcal{S}_t(\varphi, T)$:

$$\mathcal{S}_t(\varphi, \mathcal{G}_T) = f\Big(\mathcal{S}_t(\varphi, T)\Big).$$

Consider a natural isometry (Lem. 6) between the shock wave tree $S(\Psi_0)$ and either of the graphical shock trees, $\mathcal{G}^{(x,t)}(\Psi_0)$ (in the space-time domain) or $\mathcal{G}^{(x,\psi)}(\Psi_0)$ (in the phase space). The next theorem formalizes an observation that the dynamics of sinks is described by the continuous pruning (Sect. 1) of the shock wave tree.

Theorem 5 (**Annihilation pruning I**). *Suppose $g(x) \equiv 1$, and the initial potential $\Psi_0(x)$ is such that $-\Psi_0(x) \in \mathcal{E}^{\text{ex}}$ and $\Psi_0(x)$ has distinct values of local maxima. Then, the dynamics of sinks is described by the generalized dynamical pruning $\mathcal{S}_t(\varphi, \mathcal{G})$ of either the graphical tree $\mathcal{G} = \mathcal{G}^{(x,\psi)}(\Psi_0)$ (in the phase space) or $\mathcal{G} = \mathcal{G}^{(x,t)}(\Psi_0)$ (in the space-time domain), with the pruning function $\varphi(T) = \textsc{height}(T)$. Specifically, the locations of sinks at any instant $t \in [0, t_{\max})$ coincide with the location of the leaves of the pruned tree $\mathcal{S}_t(\varphi, \mathcal{G})$.*

Proof. By definition, the trajectories of the sinks coincide with the graphical tree $\mathcal{G}$ (in either phase space or space-time). Furthermore, item (c) of Lem. 5 in Sect. 6.2.3 implies that every sink travels distance t along the tree (from a leaf toward the root, according to the corresponding tree metric $d^{(x,\psi)}$ or $d^{(x,t)}$) by time t. This is equivalent to the pruning statement of the current theorem. □ □

Theorem 5 only refers to the dynamics of the sinks; it is, however, intuitively clear that the entire potential $\psi(x,t)$ at any given $t > 0$ can be uniquely reconstructed from either of the pruned graphical trees, $\mathcal{G}^{(x,t)}(\Psi_0)$ or $\mathcal{G}^{(x,\psi)}(\Psi_0)$. Because of the multiple symmetries, the graphical trees possess significant redundant information.

Next, we show that the reduced tree $\mathcal{V}(\Psi_0)$ (Cor. 3) equipped with information about the sinks provides a minimal description sufficient for reconstructing the entire continuum annihilation dynamics.

Lemma 7. *Suppose $g(x) \equiv 1$, and the initial potential $\Psi_0(x)$ is such that $-\Psi_0(x) \in \mathcal{E}^{\text{ex}}$ and $\Psi_0(x)$ has distinct values of local maxima. Then,*

$$\textsc{level}(\psi(x,t)) = \mathcal{S}_t(\textsc{length}, \mathcal{V}(\Psi_0)).$$

Proof. The statement is a part of Theorem 6 proved below. □ □

Lemma 7 states that the level set tree (i.e., the sequence of the local extreme values) of $\psi(x,t)$ is uniquely reconstructed from the pruned tree $\mathcal{V}(\Psi_0)$. This, however, is not sufficient to reconstruct the entire

time-advanced potential, which has plateaus corresponding to the intervals of zero density (recall the empty regions in the top panels of Fig. 10). The information about such plateaus is lost in the pruned tree. It happens that it suffices to remember "the size" of the pruned out parts of the tree in order to completely reconstruct the annihilation dynamics from $\mathcal{V}(\Psi_0)$. Specifically, we store the value $\varphi(\tau)$ for each subtree τ that has been pruned out. These values are stored in the *cuts* – the points where the pruned subtrees were attached to the initial tree; see Fig. 17(a). The cuts is a union of the leaves of the pruned tree and the vertices of the initial tree that became edge points in the pruned tree. A formal definition is given below.

Definition 3 (Cuts). *The set $\mathcal{D}_t(\varphi, T)$ of cuts in a pruned tree $\mathcal{S}_t(\varphi, T)$ is defined as the boundary of the pruned part of the tree*

$$\mathcal{D}_t(\varphi, T) = \partial\{x \in T \ : \ \varphi(\Delta_{x,T}) < t\}.$$

We now define an extension $\widetilde{\mathcal{S}}_t(\varphi, T)$ of the generalized dynamical pruning that preserves the sizes of pruned subtrees. Such pruning starts with a tree from $\mathcal{BL}^{|}_{\text{plane}}$ and results in a tree from the space of mass-equipped trees, denoted $\widetilde{\mathcal{BL}}^{|}_{\text{plane}}$. The pruning $\widetilde{\mathcal{S}}_t(\varphi, T)$ of a tree $T \in \mathcal{BL}^{|}_{\text{plane}}$ is a tree from $\widetilde{\mathcal{BL}}^{|}_{\text{plane}}$, whose projection to $\mathcal{BL}^{|}_{\text{plane}}$ coincides with $\mathcal{S}_t(\varphi, T)$. In addition, the tree is equipped with massive points placed at the cuts. Each massive point corresponds to a pruned out subtree τ of T, with mass equal $\varphi(\tau)$. If a cut is the boundary for two pruned subtrees (Fig. 17(a), cuts *a,d*), then it hosts two oriented masses. Such cuts are typical in prunings that do not have the semigroup property (see Fig. 8, Stage IV). Figure 17(b) illustrates mass-equipped pruning $\widetilde{\mathcal{S}}_t(\varphi, T)$ with pruning function $\varphi = \textsc{length}$.

Next, we describe how to construct the time-advanced potential $\psi_{T,t}(x)$ for a given $t \in [0, t_{\max}]$ and all $x \in [a, b]$ from a pruned mass-equipped tree $T = \widetilde{\mathcal{S}}_t(\textsc{length}, \mathcal{V}(\Psi_0))$. Theorem 6 then shows that this reconstructed potential coincides with the time-advances potential of the annihilation dynamics.

Construction 1 (Tree → potential). *Suppose $T = \widetilde{\mathcal{S}}_t(\textsc{length}, \mathcal{V}(\Psi_0))$. The corresponding potential $\psi_{T,t}(x)$, with $-\psi_{T,t}(x) \in \mathcal{E}^{\text{ex}}$, is constructed in the following steps:*

(1) *Construct the Harris path $H_T(x)$ for the projection of T to $\mathcal{BL}^{|}_{\text{plane}}$ (i.e., disregarding masses), and consider the negative excursion $-H_T(x)$.*

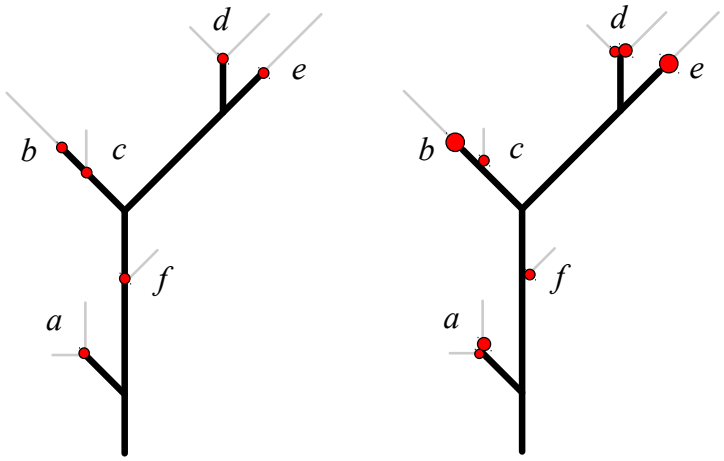

(a) Cuts (b) Massive points

FIGURE 17. Cuts and massive points: an illustration. (a) Pruned tree $\mathcal{S}_t(\textsc{length}, T)$ (solid black) with the set of cuts (red circles). The pruned parts of the initial tree T are shown in gray. Here, we prune by length; the cuts *a,d* correspond to Stage IV of Fig. 8. The cuts a and d are placed at vertices of T that became leaves within $\mathcal{S}_t(\textsc{length}, T)$. The cuts b and e are placed at the leaves of the pruned tree. The cuts c and f are placed at vertices of T that became non-vertex points within $\mathcal{S}_t(\textsc{length}, T)$. (b) Massive points (red circles) placed at the cuts. Each of the cuts a and d hosts two oriented massive points. Each of the cuts b and e hosts a single unoriented massive point. Each of the cuts c and f hosts a single oriented massive point. The circle size is proportional to the mass.

(2) *At every local minimum of* $-H_T(x)$ *that corresponds to a double mass* $(m_{\mathrm{L}}, m_{\mathrm{R}})$*, insert a horizontal plateau of length*

$$\varepsilon = 2(m_{\mathrm{L}} + m_{\mathrm{R}} - t),$$

as illustrated in Fig. 18, Stage 3.

(3) *At every monotone point of* $-H_T(x)$ *that corresponds to an internal mass* m*, insert a horizontal plateau of length* $2m$ *(Fig. 18, Stage* 2*).*

(4) *At every internal local maxima of* $-H_T(x)$*, insert a horizontal plateau of length* $2t$ *(Fig. 18, Stage* 1*).*

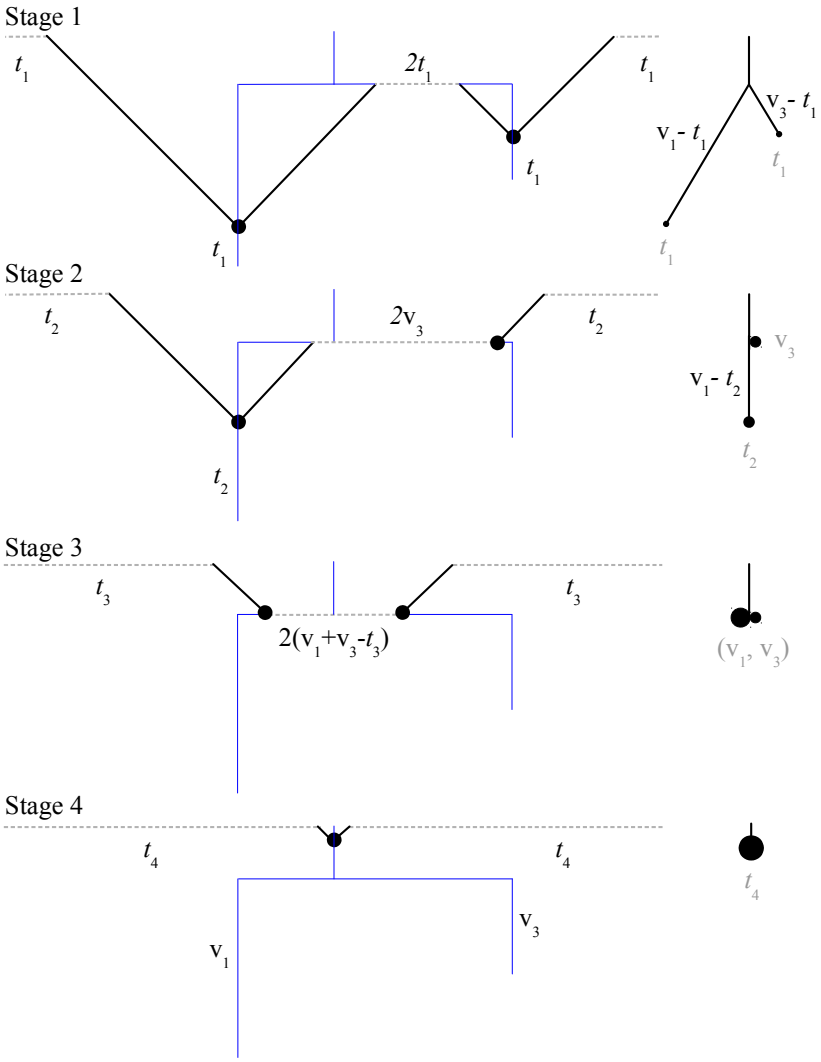

FIGURE 18. Four generic stages in the ballistic annihilation dynamics of a W-shaped potential (left), and respective mass-equipped trees (right). The lengths v_1 and v_3 of the two vertical leaf segments are assigned as illustrated in the Stage 4 (see also Fig. 15). (Left): Potential $\psi(x,t)$ is shown in solid black. Each plateau (dashed gray) corresponds to an interval of zero density. The graphical shock tree $\mathcal{G}^{(x,\psi)}(\Psi_0)$ (blue) and sinks (black circles) are shown for visual convenience. (Right): Mass-equipped trees. Segment lengths are marked in black, point masses are indicated in gray. Notice progressive increase of the point masses from Stage 1 to 4. The Stages 1 to 4 refer to time instants $t_1 < t_2 < t_3 < t_4$. Here $v_3 < v_1$, $v_3 > t_1$, $v_3 < t_2 < v_1$, $v_1 < t_3$, and $t_3 < v_1 + v_3 < t_4$.

The following theorem establishes the equivalence of the continuum annihilation dynamics and mass-equipped generalized dynamical pruning with respect to the tree length. In particular, it includes the statement of Lem. 7.

Theorem 6 (**Annihilation pruning II**). *Suppose* $g(x) \equiv 1$ *and the initial potential* $\Psi_0(x)$ *is such that* $-\Psi_0(x) \in \mathcal{E}^{\text{ex}}$ *and* $\Psi_0(x)$ *has distinct values of local maxima. Then, for any* $t \in [0, t_{\max}]$*, the time-advances potential* $\psi(x,t)$ *is uniquely reconstructed (by Construction 1) from the pruned tree* $T = \widetilde{\mathcal{S}}_t(\textit{LENGTH}, \mathcal{V}(\Psi_0))$*. That is,* $\psi(x,t) \equiv \psi_{T,t}$ *for all* $x \in [a,b]$*.*

Proof. The validity of the statement (potential reconstruction) is verified recursively, following the unfolding process of Sect. 6.2.3. Specifically, we start with a W-shaped potential for which the statement is directly verified in each of the four generic stages shown in Fig. 18. When a W-shaped potential is completely pruned, its domain is an empty interval that corresponds to an empty tree consisting of the root with a single mass equal to the interval length (end of Stage 4 in Fig. 18). Hence, the mass-equipped pruning process after that time is equivalent to that of an unfolded potential (where we replace the W-shaped potential with a V-shaped potential). This leads to the statement of the theorem. □ □

Inversely, the mass-equipped tree $\widetilde{\mathcal{S}}_t(\text{LENGTH}, \mathcal{V}(\Psi_0))$ can be uniquely reconstructed from the evolution of the time-advanced potential $\psi(x,s)$ during $s \in [0,t]$. This is done using the following construction.

Construction 2 (**Potential → tree**). *Suppose that* $-\psi(x,0) = -\Psi_0(x)$ *is a positive excursion from* $\mathcal{E}^{\text{ex}}$ *with distinct values of local minima. Then, for a fixed* $t > 0$*, a mass-equipped tree* $T_\psi(t) \in \widetilde{\mathcal{BL}}^{|}_{\text{plane}}$ *for the potential* $\psi(x,t)$ *is constructed as follows:*

(a) *The planar shape of the tree, as an element of* $\mathcal{BL}^{|}_{\text{plane}}$*, corresponds to the level set tree of the negative potential restricted to the positive density domain:* $-\psi(x,t)|_{g(x,t)>0}$*. (This corresponds, for any given* $t > 0$*, to cutting zero-density space intervals and glueing the potential segments from positive-density intervals to form a continuous positive excurison.)*
(b) *Every leaf that corresponds to a local minimum point of* $\psi(x,t)$ *is equipped with mass* $m = t$ *(Fig. 18, Stages* $1, 2, 4$*).*

(c) *Every leaf that corresponds to a local minimum plateau of length ε in $\psi(x,t)$ is equipped with a double mass $(m_{\mathrm{L}}, m_{\mathrm{R}})$ that satisfies*

$$m_{\mathrm{L}} + m_{\mathrm{R}} = \varepsilon/2 + t, \tag{26}$$

where the values of $(m_{\mathrm{L}}, m_{\mathrm{R}})$ are obtained from the evolution of $\psi(x,s)$ for $s \in [0,t]$ (Fig. 18, Stage 3).

(d) *Every internal point that corresponds to a plateau of length ε that is not a local maximum is equipped with mass $m = \epsilon/2$ (Fig. 18, Stage 2). If the plateau is located within an increasing interval of the potential $\psi(x,t)$ (decreasing interval of $-\psi(x,t)$), the mass is right-oriented (as in Fig. 18, Stage 2); if the plateau is located within a decreasing interval of the potential $\psi(x,t)$ (increasing interval of $-\psi(x,t)$), the mass is left-oriented.*

Part (c) of this construction reflects the loss of memory property of annihilation dynamics. Any pair of masses $(m_{\mathrm{L}}, m_{\mathrm{R}})$ that satisfies (26) is consistent with the model dynamics. The unique reconstruction is only possible if one knows the time-advanced potential for the entire interval $[0,t]$.

Constructions 1,2 and Thm. 6 imply that the continuum ballistic annihilation dynamics is equivalent to the mass-equipped generalized dynamical pruning of the level set tree of the initial potential. The next sections illustrates how this equivalence facilitates the analytical treatment of the model.

6.5. **Ballistic annihilation of an exponential excursion.** This section examines a special case of piece-wise linear potential with unit slopes: a negative exponential excursion. Consider potential

$$\psi(x,0) = -H_{\mathsf{GW}(\lambda)}(x)$$

that is the negative Harris path (Sect. 2.3) of an exponential critical binary Galton-Watson tree with parameter λ (Def. 2). In words, the potential is a negative finite excursion with linear segments of alternating slopes ± 1, such that the lengths of all segments except the last one are i.i.d. exponential random variables with parameter $\lambda/2$. Accordingly, the initial particle velocity $v(x,0)$ alternates between the values ± 1 at epochs of a stationary Poisson point process on $\mathbb{R}$ with rate $\lambda/2$, starting with $+1$ and until the respective potential crosses the zero level.

Corollary 4 (**Exponential excursion**). *Suppose $g(x) \equiv 1$ and initial potential $\Psi_0(x) = -H_{\mathsf{GW}(\lambda)}(x)$. Then the corresponding tree $\mathcal{V}(\Psi_0) \in \mathcal{BL}^{|}_{\mathrm{plane}}$ is an exponential binary critical Galton-Watson tree $\mathsf{GW}(\lambda)$.*

Proof. By Cor. 3, the tree $\mathcal{V}(\Psi_0)$ is the level set tree of the negative potential $-\Psi_0(x)$. The statement now follows from Thm. 1. □ □

To formulate the next result, recall that if $T \overset{d}{\sim} \mathsf{GW}(\lambda)$ and $\varphi(T) = \textsc{length}(T)$, then by (16),

$$p_t := \mathsf{P}(\varphi(T) > t) = e^{-\lambda t}\Big[I_0(\lambda t) + I_1(\lambda t)\Big].$$

Also, the p.d.f. of $\textsc{length}(T)$ is given by $\ell(x)$ of (9).

Theorem 7 (Ballistic annihilation of exponential excursion). *Suppose*
the initial particle density is constant, $g(x) \equiv 1$, and the initial potential $\psi(x, 0)$ is the negative Harris path of an exponential critical binary Galton-Watson tree with parameter λ, i.e., $\mathcal{V}(\Psi_0) \overset{d}{\sim} \mathsf{GW}(\lambda)$. Then, at any instant $t > 0$ the mass-equipped shock tree $\mathcal{V}_t = \widetilde{\mathcal{S}}_t(\textsc{length}, \mathcal{V}(\Psi_0))$ conditioned on surviving, $\mathcal{V}_t \neq \phi$, is distributed according to the following rules.

(i) *The planar shape of the tree, as an element of $\mathcal{BL}^{|}_{\text{plane}}$, is distributed as an exponential binary Galton-Watson tree $\mathsf{GW}(\lambda_t)$ with $\lambda_t := \lambda p_t$.*

(ii) *A single or double mass points are placed independently in each leaf with the probability of a single mass being*

$$\frac{2}{\lambda}\frac{\ell(t)}{p_t^2}.$$

(iii) *Each single mass at a leaf has mass $m = t$. For a double mass, the individual masses $(m_{\text{L}}, m_{\text{R}})$ have the following joint p.d.f.*

$$f(a, b) = \frac{\ell(a)\ell(b)}{p_t^2 - \frac{2}{\lambda}\ell(t)}$$

for $a, b > 0$, $a \vee b \ \leq t \ < a + b$.

(iv) *The number of mass points placed in the interior of any edge is distributed geometrically with the probability of placing k masses being*

$$p_t\Big(1 - p_t\Big)^k, \qquad k = 0, 1, 2, \ldots.$$

The locations of k mass points are independent uniform in the interior of the edge. The orientation of each mass is left or right independently with probability $1/2$.

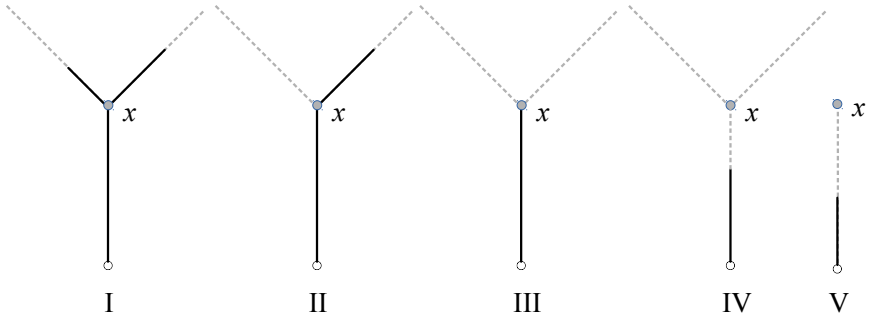

FIGURE 19. Subevents used in the proof of Theorem 7. Solid line depicts (a part of) pruned tree $\mathcal{S}_t(\varphi, T)$. Dashed line depicts (a part of) initial tree T.

(v) *The edge masses are i.i.d. random variables with the following common p.d.f.*

$$\frac{\ell(a)}{1-p_t}, \qquad a \in (0,t).$$

Proof. Part (i) follows directly from Thm. 3(a).

To establish the other parts, we first introduce a particular representation of the survival event $\mathcal{S}_t(\varphi, T) \neq \phi$, where we denote $T = \mathcal{V}(\Psi_0)$. Let X denote the length of the edge of T adjacent to the root and let x be the descendent vertex (a junction or a leaf) to the root in T. If $\mathsf{deg}_T(x) = 3$, let h_1 and h_2 represent the lengths of the two subtrees descendent from x. Then the event $\mathcal{S}_t(\varphi, T) \neq \phi$ can be written as the union of the following five non-overlapping events, illustrated in Fig. 19,

$$\begin{aligned}\Big\{\mathcal{S}_t(\varphi,T) \neq \phi\Big\} =& \{\mathsf{deg}_T(x) = 3 \ \text{ and } \ t \leq \ \mathrm{h}_1 \wedge \mathrm{h}_2\} \\ &\cup \{\mathsf{deg}_T(x) = 3 \ \text{ and } \ \mathrm{h}_1 \wedge \mathrm{h}_2 \leq \ t < \ \mathrm{h}_1 \vee \mathrm{h}_2\} \\ &\cup \{\mathsf{deg}_T(x) = 3 \ \text{ and } \ \mathrm{h}_1 \vee \mathrm{h}_2 \leq \ t < \ \mathrm{h}_1 + \mathrm{h}_2\} \\ &\cup \{\mathsf{deg}_T(x) = 3 \ \text{ and } \ \mathrm{h}_1 + \mathrm{h}_2 \leq \ t < \ X + \mathrm{h}_1 + \mathrm{h}_2\} \\ &\cup \{\mathsf{deg}_T(x) = 1 \ \text{ and } \ t < \ X\}. \end{aligned} \tag{27}$$

The probabilities of the five events in (27) are computed below.

Case I

$$\begin{aligned}\mathsf{P}(\mathsf{deg}_T(x) = 3 \ \text{ and } \ t \leq \ \mathrm{h}_1 \wedge \mathrm{h}_2) &= \frac{1}{2}\mathsf{P}(t \leq \ \mathrm{h}_1 \wedge \mathrm{h}_2 \,|\mathsf{deg}_T(x) = 3) \\ &= \frac{p_t^2}{2}. \end{aligned} \tag{28}$$

Case II

$$\begin{aligned}
&\mathsf{P}(\mathsf{deg}_T(x) = 3 \text{ and } \mathrm{h}_1 \wedge \mathrm{h}_2 \leq t < \mathrm{h}_1 \vee \mathrm{h}_2) \\
&\qquad = \frac{1}{2}\mathsf{P}(\mathrm{h}_1 \wedge \mathrm{h}_2 \leq t < \mathrm{h}_1 \vee \mathrm{h}_2 \,|\mathsf{deg}_T(x) = 3) \\
&\qquad = \mathsf{P}(\mathrm{h}_1 < t < \mathrm{h}_2 \,|\mathsf{deg}_T(x) = 3) \\
&\qquad = p_t\big(1 - p_t\big). \qquad (29)
\end{aligned}$$

Case III

$$\begin{aligned}
&\mathsf{P}(\mathsf{deg}_T(x) = 3 \text{ and } \mathrm{h}_1 \vee \mathrm{h}_2 \leq t < \mathrm{h}_1 + \mathrm{h}_2) \\
&\qquad = \frac{1}{2}\mathsf{P}(\mathrm{h}_1 \vee \mathrm{h}_2 \leq t < \mathrm{h}_1 + \mathrm{h}_2 \,|\mathsf{deg}_T(x) = 3) \\
&\qquad = \frac{1}{2}\mathsf{P}(\mathrm{h}_1 \vee \mathrm{h}_2 \leq t \,|\mathsf{deg}_T(x) = 3) - \frac{1}{2}\mathsf{P}(t < \mathrm{h}_1 + \mathrm{h}_2 \,|\mathsf{deg}_T(x) = 3) \\
&\qquad = \frac{1}{2}\big(1 - p_t\big)^2 - \frac{1}{2}F_{\mathrm{h}_1+\mathrm{h}_2}(t),
\end{aligned}$$

where

$$F_{\mathrm{h}_1+\mathrm{h}_2}(t) := \mathsf{P}(\mathrm{h}_1 + \mathrm{h}_2 < t \,|\, \mathsf{deg}_T(x) = 3) = \int_0^t \ell * \ell(y)\, dy.$$

Since $p_t = 1 - \int_0^t \ell(x)\, dx$, the Laplace transform $\mathcal{L}p(s)$ of p_t can be expressed via the Laplace transform $\mathcal{L}\ell(s)$ of $\ell(t)$ as follows:

$$\mathcal{L}p(s) = \frac{1}{s} - \int_0^\infty \int_0^t e^{-st}\ell(x)\, dx\, dt \;= \frac{1}{s} - \frac{1}{s}\mathcal{L}\ell(s).$$

Thus, by (13),

$$\mathcal{L}p(s) = \frac{1}{2s} + \frac{1}{\lambda}\mathcal{L}\ell(s) - \frac{1}{2s}\big(\mathcal{L}\ell(s)\big)^2. \qquad (30)$$

Hence, the Laplace transform of $F_{\mathrm{h}_1+\mathrm{h}_2}(t)$ is

$$\begin{aligned}
\mathcal{L}F_{\mathrm{h}_1+\mathrm{h}_2}(s) &= \frac{1}{s}\int_0^\infty e^{-st}\ell * \ell(t)\, dt = \frac{1}{s}\big(\mathcal{L}\ell(s)\big)^2 \\
&= \frac{1}{s} + \frac{2}{\lambda}\mathcal{L}\ell(s) - 2\mathcal{L}p(s).
\end{aligned}$$

Therefore,

$$F_{\mathrm{h}_1+\mathrm{h}_2}(t) = 1 + \frac{2}{\lambda}\ell(t) - 2p_t$$

and

$$\mathsf{P}(\mathsf{deg}_T(x)=3 \text{ and } \mathrm{h}_1\vee\mathrm{h}_2\le t<\mathrm{h}_1+\mathrm{h}_2)=\frac{1}{2}\Big(1-p_t\Big)^2-\frac{1}{2}F_{\mathrm{h}_1+\mathrm{h}_2}(t)$$

$$=\frac{p_t^2}{2}-\frac{1}{\lambda}\ell(t). \tag{31}$$

Case IV

$$\begin{aligned}\mathsf{P}(\mathsf{deg}_T(x)=3 \text{ and } \mathrm{h}_1+\mathrm{h}_2\le t<X+\mathrm{h}_1+\mathrm{h}_2)&\\ =\frac{1}{2}\mathsf{P}(\mathrm{h}_1+\mathrm{h}_2\le t<X+\mathrm{h}_1+\mathrm{h}_2\,|\mathsf{deg}_T(x)=3)&\\ =\frac{1}{2}\int_0^t e^{-\lambda(t-y)}\ell*\ell(y)\,dy&\\ =\frac{1}{2\lambda}\phi_\lambda*\ell*\ell(t)\quad=\frac{1}{\lambda}\ell(t)-\frac{1}{2\lambda}\phi_\lambda(t)&\end{aligned} \tag{32}$$

by (12).

Case V

$$\mathsf{P}(\mathsf{deg}_T(x)=1 \text{ and } t<X)=\frac{1}{2}\mathsf{P}(t<X)=\frac{1}{2}e^{-\lambda t}=\frac{1}{2\lambda}\phi_\lambda(t). \tag{33}$$

Observe that the probabilities in (28), (29), (31), (32), and (33) add up to

$$p_t=\mathsf{P}\Big(\mathcal{S}_t(\varphi,T)\neq\phi\Big).$$

Take a vertex v which is either an internal vertex or a root of $T=\mathcal{V}(\Psi_0)$, and select one of its descendent subtrees (there will be just one in case if v is a root). Denote it by Δ_v. Conditioning on the event $\{\mathcal{S}_t(\textsc{length},\Delta_v)\neq\phi\}$, Case III computes the probability that $\widetilde{\mathcal{S}}_t(\textsc{length},\Delta_v)$ is a leaf edge with a double mass point at the leaf vertex, while together, Case IV and Case V compute the probability that $\widetilde{\mathcal{S}}_t(\textsc{length},\Delta_v)$ is a leaf edge with a single mass point at the leaf vertex. To prove part (ii), observe that the probabilities in (32) and (33) add up to $\frac{1}{\lambda}\ell(t)$, while the probabilities in (31), (32), and (33) add up to $\frac{p_t^2}{2}$. Thus, the fraction of leaves with single sink is $\frac{1}{\lambda}\ell(t)\Big/\frac{p_t^2}{2}$.

By construction, each single mass at a leaf has mass t. For a double mass, (31) implies the following cumulative distribution function for

positive a and b satisfying $a \vee b \ \leq t \ < a + b$.

$$
\begin{aligned}
F(a,b) &= \frac{\mathsf{P}\left(\mathsf{deg}_T(x) = 3,\ \mathrm{h}_1 \leq a,\ \mathrm{h}_2 \leq b,\ t < \mathrm{h}_1 + \mathrm{h}_2 \ |\mathcal{S}_t(\varphi, T) \neq \phi\right)}{\frac{p_t^2}{2} - \frac{1}{\lambda}\ell(t)} \\
&= \frac{\int\limits_0^a \mathsf{P}\left(t - y < \mathrm{h}_2 \leq b \mid \mathcal{S}_t(\varphi, T) \neq \phi \ \text{ and } \ \mathsf{deg}_T(x) = 3\right) \ell(y)\, dy}{p_t^2 - \frac{2}{\lambda}\ell(t)} \\
&= \frac{\int\limits_0^a \Big(p_{t-y} - p_b\Big) \ell(y)\, dy}{p_t^2 - \frac{2}{\lambda}\ell(t)} \\
&= \frac{\int\limits_0^a p_{t-y}\ell(y)\, dy - p_b\Big(1 - p_a\Big)}{p_t^2 - \frac{2}{\lambda}\ell(t)}.
\end{aligned}
$$

Differentiating, we obtain the statement of part (iii):

$$
f(a,b) = \frac{\partial^2}{\partial a\, \partial b} F(a,b) = \frac{\ell(a)\ell(b)}{p_t^2 - \frac{2}{\lambda}\ell(t)}.
$$

For part (iv) observe that by (29),

(34)
$$
\mathsf{P}(\mathsf{deg}_T(x) = 3 \ \text{ and } \ \mathrm{h}_1 \wedge \mathrm{h}_2 \leq \ t < \ \mathrm{h}_1 \vee \mathrm{h}_2 \ |\mathcal{S}_t(\varphi, T) \neq \phi) = 1 - p_t.
$$

Each interior point mass in the mass-equipped shock tree $\mathcal{V}_t$ is placed at a location of an internal vertex of $T = \mathcal{V}(\Psi_0)$, where exactly one of the two descendant subtrees had been pruned out. Thus, each edge in $\mathcal{V}_t$ is partitioned into subintervals whose lengths are independent exponential random variables with parameter λ. At every point that separates a pair of adjacent subintervals there placed a mass, which can have either left or right orientation independently with probability 1/2. Equation (34) implies that the number of these subintervals in an edge of $\mathcal{V}_t$ is a geometric random variable with parameter p_t. These geometric random variables are independent from the rest of construction (i.e., exponential lengths of the subintervals, the point masses, and the combinatorial shape of $\mathcal{V}_t$).

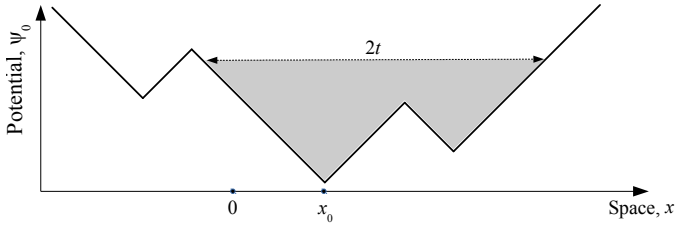

FIGURE 20. Random sink $\mathcal{M}_0$ originates at point x_0 – the local minimum closest to the origin. Its dynamics during a finite time interval $[0, t]$ is completely specified by a finite negative excursion $\mathcal{B}_0^t$ of length $2t$, similar to the one highlighted in the figure.

Finally, for $a \in (0, t)$, equation (29) implies

$$\begin{aligned}
&\frac{\mathsf{P}(\mathsf{deg}_T(x) = 3 \ \text{ and } \ \mathrm{h}_1 \wedge \mathrm{h}_2 \leq \ a < \ t < \ \mathrm{h}_1 \vee \mathrm{h}_2 \ | \mathcal{S}_t(\varphi, T) \neq \phi)}{p_t(1-p_t)} \\
&= \frac{\mathsf{P}(\mathrm{h}_1 \leq \ a < \ t < \ \mathrm{h}_2 \mid \mathcal{S}_t(\varphi, T) \neq \phi \ \text{ and } \ \mathsf{deg}_T(x) = 3)}{p_t(1-p_t)} \\
&= \frac{p_t(1-p_a)}{p_t(1-p_t)} \ = \frac{1-p_a}{1-p_t}.
\end{aligned}$$

Next, we differentiate the above probability in order to obtain the p.d.f. for the mass of an interior sink, as in part (v),

$$\frac{d}{da}\frac{1-p_a}{1-p_t} = \frac{\ell(a)}{1-p_t}.$$

□ □

6.6. **Random sink in an infinite exponential potential.** Here we focus on the dynamics of a random sink in the case of a negative exponential excursion potential. To avoid subtle conditioning related to a finite potential, we consider here an infinite exponential potential $\Psi_0^{\exp}(x)$, $x \in \mathbb{R}$, constructed as follows. Let x_i, $i \in \mathbb{Z}$ be the epochs of a Poisson point process on $\mathbb{R}$ with rate $\lambda/2$, indexed so that x_0 is the epoch closest to the origin (Fig. 20). The initial velocity $v(x, 0)$ is a piece-wise constant continuous function that alternates between values ± 1 within the intervals $(x_i - 1, x_i]$ and with $v(x_0, 0) = 1$. Accordingly, the initial potential $\Psi_0^{\exp}(x)$ is a piece-wise linear continuous function with a local minimum at x_0 and alternating slopes ± 1 of independent exponential duration. The results in this section refer to the sink $\mathcal{M}_0$ with initial Lagrangian coordinate x_0. We refer to $\mathcal{M}_0$ as a *random sink*, using translation invariance of Poisson point process.

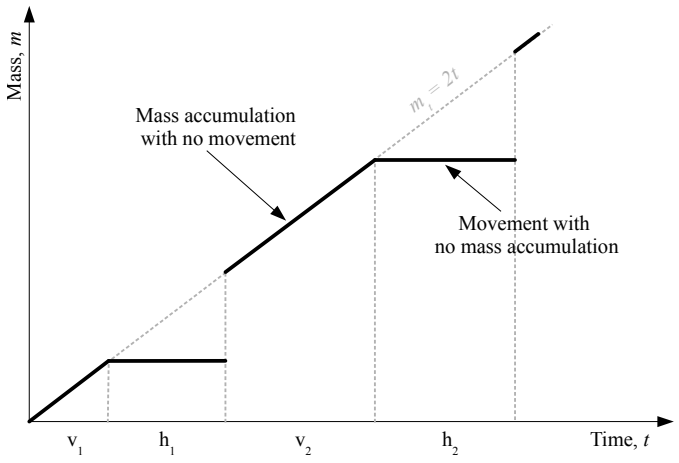

FIGURE 21. Dynamics of a random sink: an illustration. The trajectory of a sink is partitioned into alternating intervals of mass accumulation of duration v_j and intervals of movement with no mass accumulation of duration h_j. Each v_j is an exponential random variable with parameter λ. Each h_j is distributed as the total length of a critical Galton-Watson tree with exponential edge lengths with parameter λ.

Observe that for any fixed $t > 0$, the dynamics of $\mathcal{M}_0$ is completely specified by a finite non-positive excursion within $\Psi_0^{\exp}(x)$ of length $2t$ (see Fig. 20). The respective Harris path is an exponential Galton-Watson tree $\mathsf{GW}(\lambda)$. The dynamics of $\mathcal{M}_0$ consists of alternating intervals of mass accumulation (vertical segments of $\mathcal{G}^{(x,\psi)}$) and motion (horizontal segments of $\mathcal{G}^{(x,\psi)}$), starting with a mass accumulation interval. Label the lengths v_i of the vertical segments and the lengths h_i of the horizontal segments in the order of appearance in the examined trajectory. Corollary 4 implies that $\mathrm{v}_i, \mathrm{h}_i$ are independent; the lengths of v_i are i.i.d. exponential random variables with parameter λ; and the lengths of h_i equal the total lengths of independent Galton-Watson trees $\mathsf{GW}\,(\lambda)$. This description, illustrated in Fig. 21, allows us to find the mass dynamics of a random sink, which is described in the next two theorems.

Theorem 8 (**Growth probability of a random sink**). *The probability $\xi(t)$ that a random sink $\mathcal{M}_0$ is growing at a given instant $t > 0$ (that is, it is at rest and accumulates mass) is given by*

$$\xi(t) = e^{-\lambda t} I_0(\lambda t). \tag{35}$$

Proof. Let v_i, $i \geq 1$ be independent exponential random variables with parameter λ, and h_i, $i \geq 1$ be the total lengths of independent $\mathsf{GW}(\lambda)$ trees. The sum $\mathrm{v}_1 + \cdots + \mathrm{v}_k$ has the gamma density $\gamma_{\lambda,k}(x) = \frac{1}{(k-1)!}\lambda(\lambda x)^{k-1}e^{-x}$. The probability $\xi(t)$ that a random sink is growing at a given instant $t > 0$ is

$$\begin{aligned}
\xi(t) &:= \mathsf{P}(\text{ a random sink is growing at instant } t\ ) \\
&= \sum_{k=1}^{\infty} \mathsf{P}\left(\sum_{i=1}^{k-1}[\mathrm{v}_i + \mathrm{h}_i] < t < \mathrm{v}_k + \sum_{i=1}^{k-1}[\mathrm{v}_i + \mathrm{h}_i]\right) \\
&= \sum_{k=1}^{\infty} \int_0^t \left(\int_{t-x}^{\infty} \lambda e^{-\lambda y} dy\right) \gamma_{k-1} * \ell_{k-1}(x)dx \\
&= \sum_{k=1}^{\infty} \int_0^t e^{-\lambda(t-x)} \gamma_{k-1} * \ell_{k-1}(x)dx \ = \frac{1}{\lambda}\sum_{k=1}^{\infty} \gamma_k * \ell_{k-1}(t), \qquad (36)
\end{aligned}$$

where

$$\ell_k(x) = \underbrace{\ell * \ldots * \ell}_{k \text{ times}}(x).$$

We calculate the Laplace transform $\mathcal{L}\xi(s)$ of the probability $\xi(t)$ in (36) as follows. We use the formula for the Laplace transform of $\ell(x)$ derived in (11) and (36) to obtain

$$\begin{aligned}
\mathcal{L}\xi(s) &= \frac{1}{\lambda}\sum_{k=1}^{\infty}\left(\frac{\lambda}{\lambda+s}\right)^k \Big(\mathcal{L}\ell(s)\Big)^{k-1} = \frac{1}{\lambda + s - \lambda\mathcal{L}\ell(s)} \\
&= \frac{1}{\lambda + s - \frac{\lambda^2}{\lambda+s+\sqrt{(\lambda+s)^2-\lambda^2}}} = \frac{1}{\sqrt{(\lambda+s)^2-\lambda^2}}. \qquad (37)
\end{aligned}$$

Finally, we use formula 29.3.93 in [2] to invert the Laplace transform in (37), and obtain

$$\xi(t) = e^{-\lambda t} I_0(\lambda t).$$

□ □

Theorem 9 (Mass distribution of a random sink). *The mass of a random sink $\mathcal{M}_0$ at instant $t > 0$ has probability distribution*

$$\begin{aligned}
\mu_t(da) = \frac{\lambda}{2}e^{-\lambda t}\Big[I_0\big(\lambda(t-a/2)\big) + I_1\big(\lambda(t-a/2)\big)\Big] I_0(\lambda a/2)\cdot \mathbf{1}_{(0,2t)}(a)da \\
+ e^{-\lambda t} I_0(\lambda t)\delta_{2t}(da), \qquad (38)
\end{aligned}$$

where δ_{2t} denotes Dirac delta function (point mass) at $2t$.

Proof. Let m_t denote the mass of a random sink at a fixed instant $t > 0$. When the sink is not growing, its mass m_t is strictly smaller than $2t$. Then for any positive $a < 2t$,

$$\begin{aligned}\mathsf{P}(m_t \le a) &= \sum_{k=1}^{\infty} \mathsf{P}\left(-\mathrm{h}_k + \sum_{i=1}^{k}[\mathrm{v}_i + \mathrm{h}_i] \ \le \frac{a}{2} < t < \sum_{i=1}^{k}[\mathrm{v}_i + \mathrm{h}_i]\right)\\ &= \sum_{k=1}^{\infty} \int_0^{a/2} \left(\int_{t-x}^{\infty} \ell(y)dy\right) \gamma_k * \ell_{k-1}(x)dx,\end{aligned}$$

and the corresponding density will be

$$\begin{aligned}\frac{d}{da}\mathsf{P}(m_t \le a) &= \frac{1}{2}\int_{t-a/2}^{\infty} \ell(y)dy \cdot \sum_{k=1}^{\infty} \gamma_k * \ell_{k-1}(a/2)\\ &= \frac{\lambda}{2}\int_{t-a/2}^{\infty} \ell(y)dy \cdot \xi(a/2)\\ &= \frac{\lambda}{2}e^{-\lambda(t-a/2)}\Big[I_0\big(\lambda(t-a/2)\big) + I_1\big(\lambda(t-a/2)\big)\Big] \cdot e^{-\lambda a/2} I_0(\lambda a/2)\\ &= \frac{\lambda}{2}e^{-\lambda t}\Big[I_0\big(\lambda(t-a/2)\big) + I_1\big(\lambda(t-a/2)\big)\Big] \cdot I_0(\lambda a/2)\end{aligned}$$

by (16) and (35). Thus, the distribution of the mass of a random sink at instant t is given by

$$\begin{aligned}\mu_t(da) =& \mathbf{1}_{(0,2t)}(a) \cdot \frac{d}{da}\mathsf{P}(m_t \le a)\, da + \xi(t)\delta_{2t}(da)\\ =& \frac{\lambda}{2}e^{-\lambda t}\Big[I_0\big(\lambda(t-a/2)\big) + I_1\big(\lambda(t-a/2)\big)\Big] I_0(\lambda a/2) \cdot \mathbf{1}_{(0,2t)}(a)da\\ &+ e^{-\lambda t} I_0(\lambda t)\delta_{2t}(da),\end{aligned}$$

where δ_{2t} denotes Dirac delta function (point mass) at $2t$. □ □

Remark 2. One can notice that the continuum annihilation dynamics of this section, with its shock waves, shock wave trees, and massive points is reminiscent of that in the 1-D inviscid Burgers equation that describes the evolution of the velocity field $v(x,t)$:

$$\partial_t v(x,t) + v(x,t)\,\partial_x v(x,t) = 0, \quad x \in \mathbb{R}, t \in \mathbb{R}_+. \tag{39}$$

The Burgers dynamics appears in a surprising variety of problems, ranging from cosmology to fluid dynamics and vehicle traffic models; see [6, 24, 26] for comprehensive review. The solution of the Cauchy problem for the Burgers equation develops singularities (shocks) that correspond to intersection of individual particles. The shocks evolve

via the shock waves that can be described as massive particles that aggregate the colliding regular particles and hence accumulate the mass of the media. The dynamics of these massive particles generates a tree structure for their world trajectories, the shock wave tree [12, 26].

The case of smooth random initial velocity can be treated explicitly via the Hopf-Cole solution. The case of non-smooth random initial velocities, e.g. a white noise or a (fractional) Brownian motion, has been extensively studied, both numerically [43] and analytically [45, 11, 12, 25]. In this case, tracing the dynamics of the massive particles backward in time (from a point within a shock tree to the leaves) corresponds to fragmentation of the mass and describes the genealogy of the shocks, i.e., the sets of particles that merge with a given massive particle [10, 25]. In particular, Bertoin [12] established that the shock wave tree for a Brownian motion initial velocity becomes the eternal additive coalescent after a proper time change; similar arguments apply for the Lévy type initial velocities [37].

7. Real trees

Recall that a metric space (X, d) is called 0-hyperbolic, if any quadruple $w, x, y, z \in X$ satisfies the following *four point condition* [21, Lemma 3.12]:

$$d(w,x) + d(y,z) \le \max\{d(w,y) + d(x,z), d(x,y) + d(w,z)\}. \tag{40}$$

The four point condition is an algebraic description of an intuitive geometric constraint on geodesic connectivity of quadruples that is shown in Fig. 22(a). An equivalent way to define 0-hyperbolicity is the three point condition illustrated in Fig. 22(b); it states that any triangle is a tripod. It is readily seen that the four point condition is satisfied by any finite tree with edge lengths (considered as a metric space with segment lengths induced by the edge lengths). In general, a connected and 0-hyperbolic metric space is called a *real tree*, or $\mathbb{R}$-tree [21, Theorem 3.40]. We denote a real tree by (T, d), referring to the underlying space T and metric d, respectively. A real tree (T, d) is *geodesically linear*, which means that for any two points $x, y \in T$ there exists a unique segment (an isometry image) within T with endpoints $\{x, y\}$ [21, Definition 3.2]. We denote this segment by $[x, y] \subset T$. A real tree is called *rooted* if one of its points, denoted here by ρ_T, is selected as the tree root. Similarly to the case of finite trees, we say that a point $p \in T$ is an *ancestor* of point $q \in T$ if the segment with endpoints q and ρ includes p: $p \in [q, \rho] \subset T$. In this case, the point q is called a *descendant* of point p. We denote by $\Delta_{p,T}$ the descendant tree at point p, that is the set of all descendants of point $p \in T$, including p as the

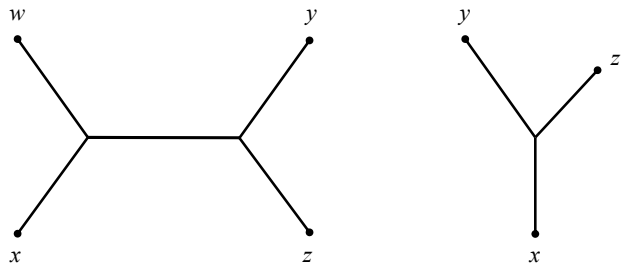

(a) Four point condition (b) Three point condition

FIGURE 22. Equivalent conditions for 0-hyperbolicity of a metric space (X, d). (a) Four point condition: any quadruple $w, x, y, z \in X$ is geodesically connected as shown in the figure. This configuration is algebraically expressed in Eq. (40). (b) Three point condition: any triplet $x, y, z \in X$ is geodesically connected as shown in the figure (i.e., any triangle is a tripod).

tree root. The set of all descendant leaves of point p is denoted by $\Delta^{\circ}_{p,T}$.

7.1. **Real tree description of ballistic annihilation.** We construct here (Sect. 7.1.1) an $\mathbb{R}$-tree $\mathbb{T} = \mathbb{T}(\Psi_0)$ that describes the entire model dynamics as coalescence of particles and sinks; this tree is sketched by gray lines in the top panel of Figs. 10 and 23. Specifically, the tree consists of points (x, t) such that there exist either a particle or a sink with coordinate x at time t. There is one-to-one correspondence between the initial particles $(x, 0)$ and leaf vertices of $\mathbb{T}$. Each leaf edge of $\mathbb{T}$ corresponds (one-to-one) to the free (ballistic) run of a corresponding particle before annihilating in a sink. Four of such free runs are depicted by green arrows in Fig. 23. The shock wave tree (movement and coalescence of sinks) corresponds to the non-leaf part of the tree $\mathbb{T}$; it is shown by blue lines in Figs. 10, 23. We adopt a convention that the motion of a particle consists of two parts: an initial ballistic run at unit speed, and subsequent motion within a respective sink. For example, the within-sink motion of particles x and x' is shown by red line in Fig. 23. This interpretation extends motion of all particles to the same time interval $[0, t_{\max}]$, with $t_{\max}$ being the time when the last remaining sink accumulates the total mass on the initial interval. This final sink serves as the tree root. Section 7.1.1 introduces a proper metric on this space so that the model is represented by a time oriented

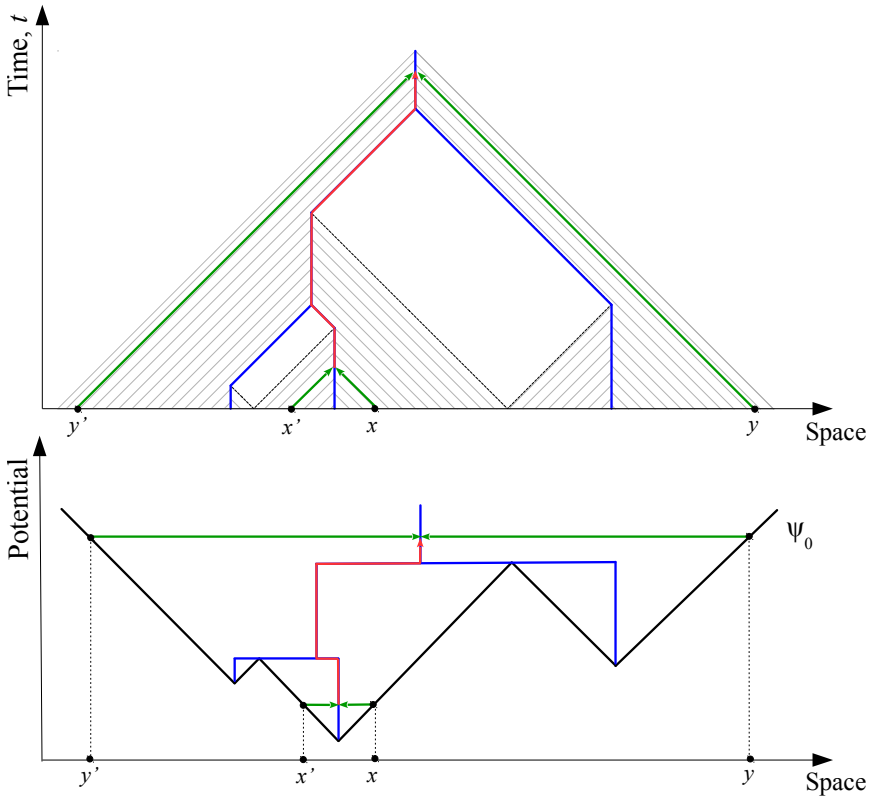

FIGURE 23. $\mathbb{R}$-tree representation of a ballistic annihilation model with a unit slope potential: an illustration. Figure illustrates dynamics of four points, x, x', y, and y', marked in the horizontal space axis. The pairs of points $\{x, x'\}$ and $\{y, y'\}$ collide and annihilate with each other. Green arrows correspond to ballistic runs of points x, x', y, y', and hence to leaves of tree $\mathbb{T}(\Psi_0)$. Red line corresponds to the trajectory of points x, x' after their collision, within a sink. The rest of notations are the same as in Fig. 10.

rooted $\mathbb{R}$-tree. In particular, the metric induced by this tree on the initial particles $(x, 0)$ becomes an *ultrametric*, with the distance between any two particles equal to the time until their collision (as particles or as respective sinks).

7.1.1. $\mathbb{R}$*-tree representation of ballistic annihilation.* We construct here a real tree representation of the continuum ballistic annihilation model of Sect. 6. Specifically, we assume a unit particle density $g(x) \equiv 1$ and initial potential $-\Psi_0(x) \equiv -\psi(x, 0) \in \mathcal{E}^{\mathrm{ex}}$, i.e. $\Psi_0(x)$ is a unit

slope negative excursion with a finite number of segments on a finite interval $[a, b]$ (e.g., bottom panel of Fig. 10). Recall that the interval $[a, b]$ completely annihilates by time $t_{\max} = (b-a)/2$, producing a single sink at space-time location $((b + a)/2, t_{\max})$.

Consider the model's entire space-time domain $\mathbb{T} = \mathbb{T}(\Psi_0)$ that consists of all points of the form (x, t), $x \in [a, b]$, $0 \le t \le t_{\max}$, such that there exists either a particle or a sink at location x at time instant t. The shaded (hatched) regions in the top panels of Figs. 10,15 are examples of such sets of points. For any pair of points (x, t) and (y, s) in $\mathbb{T}$, we define their unique *earliest common ancestor* as a point

$$\mathsf{A}_{\mathbb{T}}((x, t), (y, s)) = (z, w) \in \mathbb{T}$$

such that w is the infimum over all w' such that

$$\exists\, z' \,:\, \{(x, t), (y, s)\} \in \Delta_{(z',w'),\mathbb{T}}.$$

The length of the unique segment between the points (x, t) and (y, s) is defined as

$$d\Big((x, t), (y, s)\Big) = \frac{1}{2}\Big((w - t) + (w - s)\Big) = \frac{1}{2}(2w - s - t), \tag{41}$$

where w is the time component of $(z, w) = \mathsf{A}_{\mathbb{T}}((x, t), (y, s))$.

The tree $(\mathbb{T}, d)$ for a simple initial potential is illustrated in the top panel of Fig. 10 by gray lines. The tree has a relatively simple structure. There is a one-to-one correspondence between the initial particles $(x, 0)$, $x \in [a, b]$, and the leaf vertices of $\mathbb{T}$. There is a one-to-one correspondence between the ballistic runs of the initial particles (runs before collision and annihilation) and the leaf edges of $\mathbb{T}$. Four of such runs are shown by green arrows in Fig. 23. There is one-to-one correspondence between the sink points $(\sigma(t), t)$ and the non-leaf part of $\mathbb{T}$. In particular, the tree root corresponds to the final sink $((a+b)/2, t_{\max})$. The sink points are shown by blue line in Figs. 10,15. It is now straightforward to check that the tree $(\mathbb{T}, d)$ satisfies the four point condition.

Consider again the sink subspace of $\mathbb{T}$, which consists of the points $\{\sigma(t), t)\}$ such that there exists a sink at location $\sigma(t)$ at time instant t, equipped with the distance (41). This metric subspace is also a tree, as a connected subspace of an $\mathbb{R}$-tree [21]. This tree is isometric to the shock wave tree $S(\Psi_0)$ and hence to either of its graphical representations $\mathcal{G}^{(x,t)}(\Psi_0)$ or $\mathcal{G}^{(x,\psi)}(\Psi_0)$ that are illustrated in Figs. 10,15 (top and bottom panels, respectively).

From the above construction, it follows that all leaves $(x, 0)$ are located at the same depth (distance from the root) $t_{\max}$. To see this, consider the segment that connect a leaf and the root and apply (41). Moreover, each *time section* at a fixed instant t_0, $\mathsf{sec}(\mathbb{T}, t_0) = \{(x, t_0) \in$

$\mathbb{T}\}$, is located at the same depth $t_{\max} - t_0$. This implies, in particular, that for any fixed $t_0 \geq 0$, the metric induced by $\mathbb{T}$ on $\mathsf{sec}(\mathbb{T}, t_0)$ is an *ultrametric*, which means that $d_1(p,q) \leq d_1(p,r) \vee d_1(r,q)$ for any triplet of points $p, q, r \in \mathsf{sec}(\mathbb{T}, t_0)$. Accordingly, each triangle $p, q, r \in \mathsf{sec}(\mathbb{T}, t_0)$ is an *isosceles*, meaning that at least two of the three pairwise distances between p, q and r are equal and not greater than the third [21, Def. 3.31]. The length definition (41) implies that the distance between any pair of points from any fixed section $\mathsf{sec}(\mathbb{T}, t_0)$ equals the time until the two points (each of which can be either a particle or a sink) collide.

We notice that the collection of leaf vertices $\Delta^\circ_{p,\mathbb{T}}$ descendant to a point $p \in \mathbb{T}$ can be either a single point $(x_p, 0)$, if p is within a leaf edge and represents the ballistic run of a particle, or an interval $\{(x,0) : x_{\text{left}}(p) \leq x \leq x_{\text{right}}(p)\}$, if p is a non-leaf point that represents a sink. We define the *mass* $m(p)$ of a point $p \in \mathbb{T}$ as

$$m(p) = \int\limits_{x:(x,0)\in\Delta^\circ_{p,\mathbb{T}}} g(z)dz = x_{\text{right}}(p) - x_{\text{left}}(p),$$

where the last equality reflects the assumption $g(z) \equiv 1$. The mass $m(p)$ generalizes the quantity "number of descendant leaves" (Sect. 4) to the $\mathbb{R}$-tree situation with an uncountable set of leaves. We observe that (i) a point $p \in \mathbb{T}$ represents a ballistic run if and only if $m(p) = 0$; (ii) a point $p \in \mathbb{T}$ represents a sink if and only if $m(p) > 0$. This means that the shock wave tree, which is isometric to the sink part of the tree $(\mathbb{T}, d)$, can be extracted from $(\mathbb{T}, d)$ by the condition $\{p : m(p) > 0\}$.

7.2. **Metric spaces on the set of initial particles.** In this section we discuss two metrics on the system's domain $[a, b]$, which is isometric to the set $\{(x,0) : x \in [a,b]\}$ of initial particles. These metrics contain the key information about the system dynamics and, unlike the complete tree $(\mathbb{T}, d)$ of Sect. 7.1.1, can be readily constructed from the potential $\Psi_0(x)$. One of these descriptions is an $\mathbb{R}$-tree and the other is not.

Metric $h_1(x,y)$ reproduces the ultrametric induced by $(\mathbb{T}, d)$ on $[a, b]$. Below we explicitly connect this metric to $\Psi_0(x)$. For any pair of points $x, y \in [a, b]$ we define a basin $\mathsf{B}_{\Psi_0}(x, y)$ as the interval that supports the minimal negative excursion within $\Psi_0(x)$ that contains the points x, y. Formally, assuming without loss of generality that $x < y$ we find the maximum of Ψ_0 on $[x, y]$:

$$\mathsf{m}_{\Psi_0}(x,y) = \sup_{z\in[x,y]} \Psi_0(z)$$

and use it to define the basin $\mathsf{B}_{\Psi_0}(x,y) = [l,r]$, where

$$l = \sup\{z : z \le x, \Psi_0(z) \ge \mathsf{m}_{\Psi_0}(x,y)\},$$
$$r = \inf\{z : z \ge y, \Psi_0(z) \ge \mathsf{m}_{\Psi_0}(x,y)\}.$$

The metric is now defined as

$$h_1(x,y) = \frac{1}{2}|\mathsf{B}_{\Psi_0(x,y)}|.$$

It is straightforward to check that

$$h_1(x,y) = \text{the time until collision of the particles } (x,0) \text{ and } (y,0),$$

where the collision is understood as either collision of particles, collision of sinks that annihilated the particles, or collision between a sink that annihilated one of the particles and the other particle. For instance, the claim is readily verified, by examining the bottom panel of Fig. 23, for any pair of points from the set $\{x, x', y, y'\}$. The metric space $([a,b], h_1)$ is not a tree. Moreover, this space is *totally disconnected*, since there only exists a finite number of points (local minima of $\Psi_0(x)$) that have a neighborhood of arbitrarily small size. Any other point at the Euclidean distance ϵ from the nearest local minimum is separated from other points by at least $\epsilon/2$.

Metric $h_2(x,y)$ describes the mass accumulation by sinks during the annihilation process. Specifically, we introduce an equivalence relation among the annihilating particles, by writing $x \sim_{\Psi_0} y$ if the particles with initial coordinates x and y collide and annihilate with each other. For example, in Fig. 23 we have $x \sim_{\Psi_0} x'$ and $y \sim_{\Psi_0} y'$. The following metric is now defined on the quotient space $[a,b]|_{\sim_{\Psi_0}}$:

$$h_2(x,y) = 2 \sup_{z \in [x,y]} [\Psi_0(z)] - \Psi_0(x) - \Psi_0(y).$$

In words, the distance $h_2(x,y)$ between particles x and y equals the total mass accumulated by the sinks to which the particles belong during the time intervals between the instants when the particles joined the respective sinks and the instant of particle (or respective sink) collision. Another interpretation is that $h_2(x,y)$ equals to the minimal Euclidean distance between points $x, y \in [a,b]|_{\sim_{\Psi_0}}$ in the quotient space; one can travel in this quotient space as along a regular real interval, with a possibility to jump (with no distance accumulation) between equivalent points.

We observe that metric $h_2(x,y)$ coincides with that of Eq. (1). Hence, the metric space $([a,b]|_{\sim_{\Psi_0}}, h_2)$ is a tree that is isometric to the level set tree of the potential $\Psi_0(x)$ on $[a,b]$ and hence to the (finite) shock wave tree $\mathcal{V}(\Psi_0)$ (by Cor. 3), with the convention that the root is placed in

$a \sim_{\Psi_0} b$. This means, in particular, that prunings of these two trees, with the same pruning function and pruning time, coincide.

7.3. **Other prunings on $\mathbb{T}$.** One can introduce a large class of prunings on an $\mathbb{R}$-tree $(\mathbb{T}, d)$ following the approach used above to define the point mass $m(p)$. Specifically, consider a measure $\eta(\cdot)$ on $[a, b]$ and define $m_\eta(p) = \eta(\Delta^\circ_{p,\mathbb{T}})$. The function $m_\eta(p)$ is nondecreasing along each segment that connect a leaf and the root $\rho_\mathbb{T}$ of $\mathbb{T}$. Hence, one can define a pruning with respect to m_η on $\mathbb{T}$ by cutting all points p with $m_\eta(p) < t$ for a given $t \geq 0$. It is readily seen that the function $m_\eta(p)$ typically has discontinuities along a path between a leaf and the root of $\mathbb{T}$. This means that pruning with respect to m_η typically does not have the semigroup property.

8. Discussion

This paper introduces a generalized dynamical pruning of rooted trees (Sect. 3) that encompasses several pruning operations discussed in the probability literature, notably including the tree erasure from leaves at a constant rate of Example 1 [38, 21, 15] and Horton pruning of Example 2 [40, 14, 33, 34]. Curiously, these two examples seem to be the only cases when the pruning satisfies the semigroup property (either in discrete or continuous time). The other natural pruning operations, like pruning by the total tree length (Example 3) or by the number of leaves (Example 4), do not have the semigroup property. The absence of semigroup property is related to the existence of discontinuities of a respective pruning function $\varphi(T)$ along a tree $T \in \mathcal{L}_{\text{plane}}$. It would be interesting to find the necessary and sufficient conditions on $\varphi(T)$ for the existence or absence of the semigroup property.

The presented results naturally complement an existing modeling framework for finite binary self similar trees [31, 32, 33], and are tailored for a particular application – continuum ballistic annihilation model – considered in this work (Sect. 5,6). However, the generalized dynamical pruning is readily applicable to more general $\mathbb{R}$-trees as discussed in Sect. 7. For instance, continuum ballistic annihilation with a general continuous potential is a natural object to be studies in a real tree framework.

Pruning might play a role in the analysis of dynamical systems, including the problem of finding self-similar or time-invariant solutions. We show here (Sect. 6) that the dynamics of a ballistic annihilation model $A + A \to \varnothing$, well known in the physics literature, is equivalent to the generalized dynamical pruning of a level set tree representation

of the model potential (Sect. 6.4, Thm. 6). This tree-based representation of the model dynamics opens a way to a complete probabilistic description of model solutions (Sect. 6.5, Thm. 7), and finding the time evolution of selected statistics (Sect. 6.6, Thms. 8,9). It seems promising to expand the proposed analysis to other initial potentials, as well as to other particle systems known to be critically dependent on the shock dynamics.

Tree measures invariant with respect to the generalized pruning (Sect. 3.4, Def. 1) are abundant in $\mathcal{BL}_{\text{plane}}$. A natural example is the critical binary Galton-Watson tree $\mathsf{GW}(\lambda)$ with i.i.d. exponential edge lengths, which is a traditional subject of invariance studies [34]. This tree is shown here to be prune invariant under arbitrary choice of the pruning function (Sect. 4.3, Thm. 2). The work [33] introduces a *Hierarchical Branching Process* (HBP) that induces a variety of measures invariant with respect to the Horton pruning. It is very likely that the approach used to construct the HBP can be used to construct measures invariant with respect to other versions of the generalized dynamical pruning. An interesting problem is finding measures invariant with respect to multiple versions of pruning. At the moment the only known solution is the exponential critical binary Galton-Watson tree $\mathsf{GW}(\lambda)$, invariant with respect to all admissible prunings. It seems that a family of *critical Tokunaga trees*, which is a one-parametric subclass of the HBP [33], is a promising candidate to be invariant with respect to other prunings.

Acknowledgements

We are grateful to Maxim Arnold for numerous discussions related to this work and to Ed Waymire for his continuing support and encouragement. We would like to thank two anonymous referees for their positive feedback and constructive comments that helped to improve the initial version of this work. This research is supported by the NSF awards DMS-1412557 (Y.K.) and EAR-1723033 (I.Z.), and by FAPESP award 2018/07826-5 (Y.K).

References

[1] R. Abraham, J.-F. Delmas, H. He, *Pruning Galton-Watson trees and tree-valued Markov processes* Ann. Inst. H. Poincaré Probab. Statist., **48**(3) (2012) 688–705.

[2] M. Abramowitz and I. A. Stegun, *Handbook of mathematical functions: with formulas, graphs, and mathematical tables* Courier Corporation, **55** (1964).

[3] D. J. Aldous, *The continuum random tree I.* The Annals of Probability, **19**(1) (1991) 1–28.

[4] D. J. Aldous, *The continuum random tree III.* The Annals of Probability, **21**(1) (1993) 248-289.
[5] D.J. Aldous, J. Pitman, *Tree-valued Markov chains derived from Galton-Watson processes* Ann. Inst. H. Poincaré Probab. Statist., **34**(5) (1998) 637–686.
[6] J. Bec and K. Khanin, *Burgers turbulence* Physics Reports, **447**(1) (2007) 1–66.
[7] E. Ben-Naim, S. Redner, and F. Leyvraz, *Decay kinetics of ballistic annihilation* Physical Review Letters, **70**(12) (1993) 1890–1893.
[8] E. Ben-Naim, S. Redner, and P. L. Krapivsky, *Two scales in asynchronous ballistic annihilation* J. Phys. A: Math. Gen., **29** L561 (1996).
[9] V. Belitsky and P. A. Ferrari, *Ballistic annihilation and deterministic surface growth* Journal of Statistical Physics, **80**(3-4) (1995) 517–543.
[10] F. Bernardeau and P. Valageas, *Merging and fragmentation in the Burgers dynamics* Phys. Rev. E, **82**:016311 (2010).
[11] J. Bertoin, *The inviscid Burgers equation with Brownian initial velocity* Comm. Math. Phys. **193**(2) (1998) 397–406.
[12] J. Bertoin, *Clustering statistics for sticky particles with Brownian initial velocity* Journal de Mathématiques Pures et Appliquées, **79**(2) (2000) 173–194.
[13] R. A. Blythe, M. R. Evans, and Y. Kafri, *Stochastic ballistic annihilation and coalescence* Physical Review Letters, **85**(18) (2000) 3750–3753.
[14] G. A. Burd, E. C. Waymire and R. D. Winn, *A self-similar invariance of critical binary Galton-Watson trees* Bernoulli, **6** (2000) 1–21.
[15] T. Duquesne and M. Winkel, *Hereditary tree growth and Levy forests* Stochastic Processes and their Applications, Vol. **129**(10), (2019) 3690–3747
[16] P. S. Dodds, D. H. Rothman, *Unified view of scaling laws for river networks* Phys. Rev. E, **59**(5) (1999) 4865.
[17] M. Droz, P.-A. Rey, L. Frachebourg, and J. Piasecki, *Ballistic-annihilation kinetics for a multivelocity one-dimensional ideal gas* Phys. Rev. E **51**(6) (1995) 5541–5548.
[18] Y. Elskens and H. L. Frisch, *Annihilation kinetics in the one-dimensional ideal gas* Physical Review A, **31**(6) (1985) 3812–3816.
[19] A. Ermakov, B. Toth, and W. Werner, *On some annihilating and coalescing systems* Journal of Statistical Physics, **91**(5-6) (1998) 845–870.
[20] A. P. Ershov, *On programming of arithmetic operations* Communications of the ACM, **1** no. 8 (1958), 3–6.
[21] S. N. Evans, *Probability and real trees: Ecole d'été de probabilités de Saint-Flour* Lectures on Probability Theory and Statistics. Springer (2008).
[22] S. N. Evans, J. Pitman, and A. Winter, *Rayleigh processes, real trees, and root growth with re-grafting* Probability Theory and Related Fields **134**(1) (2006) 81–126.
[23] P. Flajolet, J.-C. Raoult, J. Vuillemin, *The number of registers required for evaluating arithmetic expressions* Theoretical Computer Science **9**(1) (1979) 99–125.
[24] U. Frisch, J. Bec, and B. Villone, *Singularities and the distribution of density in the Burgers/adhesion model* Physica D, **152/153** (2001) 620–635.
[25] C. Giraud, *Genealogy of shocks in Burgers turbulence with white noise initial velocity* Comm. Math.Phys., **223**, (2001) 67–86.

[26] S. Gurbatov, A. Malakhov, and A. Saichev, *Nonlinear random waves and turbulence in nondispersive media: waves, rays, particles* Manchester University Press, Manchester, (1991)

[27] T. E. Harris, *First passage and recurrence distribution* Trans. Amer. Math. Soc., **73** (1952) 471–486.

[28] A. Katok and B. Hasselblatt, *Introduction to the modern theory of dynamical systems* Vol. 54. Cambridge university press (1997).

[29] J. W. Kirchner, *Statistical inevitability of Horton's laws and the apparent randomness of stream channel networks* Geology, **21**(7) (1993) 591–594.

[30] Y. Kovchegov and I. Zaliapin, *Horton Law in Self-Similar Trees* Fractals, Vol. 24, No. 2 (2016) 1650017.

[31] Y. Kovchegov and I. Zaliapin, *Horton self-similarity of Kingman's coalescent tree* Ann. Inst. H. Poincaré Probab. Statist., **53**(3) (2017) 1069–1107.

[32] Y. Kovchegov and I. Zaliapin, *Tokunaga self-similarity arises naturally from time invariance* Chaos: An Interdisciplinary Journal of Nonlinear Science, 28(4) (2018) 041102.

[33] Y. Kovchegov and I. Zaliapin, *Random self-similar trees and a hierarchical branching process* Stochastic Processes and Their Applications, **129**(7) (2019) 2528–2560, doi:10.1016/j.spa.2018.07.015

[34] Y. Kovchegov and I. Zaliapin, *Random Self-Similar Trees: A mathematical theory of Horton laws* Probability Surveys, **17**(0) (2020) 1–213. https://doi.org/10.1214/19-PS331

[35] P. L. Krapivsky, S. Redner, and E. Ben-Naim, *A kinetic view of statistical physics* Cambridge University Press (2010).

[36] J. F. Le Gall, *The uniform random tree in a Brownian excursion* Probab. Theory Relat. Fields, **96** (1993) 369–383.

[37] G. Miermont, *Ordered additive coalescent and fragmentations associated to Lévy processes with no positive jumps* Electronic Journal of Probability, Vol. **6** (2001), paper no. 14, 1–33.

[38] J. Neveu, *Erasing a branching tree* Advances in applied probability, **1** (1986) 101–108.

[39] J. Neveu and J. Pitman, *Renewal property of the extrema and tree property of the excursion of a one-dimensional Brownian motion* Séminaire de Probabilités XXIII, **1372** of the series Lecture Notes in Mathematics, (1989) 239–247.

[40] S. D. Peckham, *New results for self-similar trees with applications to river networks* Water Resources Res. **31** (1995) 1023–1029.

[41] J. Piasecki, *Ballistic annihilation in a one-dimensional fluid* Phys.Rev. E **51**(6) (1995) 5535–5540.

[42] J. Pitman, *Combinatorial Stochastic Processes: Ecole d'été de probabilités de Saint-Flour XXXII-2002* Lectures on Probability Theory and Statistics. Springer (2006).

[43] Z.-S. She, E. Aurell, and U. Frisch, *The inviscid Burgers equation with initial data of Brownian type* Comm. Math. Phys., **148**(3) (1992), 623–641.

[44] V. Sidoravicius and L. Tournier, *Note on a one-dimensional system of annihilating particles* Electron. Commun. Probab., **22**(59) (2017) 1–9.

[45] Y. G. Sinai, *Statistics of shocks in solutions of inviscid Burgers equation* Comm. Math. Phys., **148**(3) (1992) 601–621.

[46] D. G. Tarboton, *Fractal river networks, Horton's laws and Tokunaga cyclicity* Journal of hydrology, **187**(1) (1996) 105–117.
[47] I. Zaliapin and Y. Kovchegov, *Tokunaga and Horton self-similarity for level set trees of Markov chains* Chaos, Solitons & Fractals, **45**(3) (2012) 358–372.
[48] S. Zanardo, I. Zaliapin, and E. Foufoula-Georgiou, *Are American rivers Tokunaga self-similar? New results on fluvial network topology and its climatic dependence* J. Geophys. Res., **118** (2013) 166–183.

Department of Mathematics, Oregon State University, Corvallis, OR, USA
Email address: kovchegy@math.oregonstate.edu

Department of Mathematics and Statistics, University of Nevada, Reno, NV, USA
Email address: zal@unr.edu